1995-09

Remote sensing and validation of surface currents from HF radar

Melton, Darryl C.

Monterey, California. Naval Postgraduate School

NAVAL POSTGRADUATE SCHOOL
MONTEREY, CALIFORNIA

THESIS

REMOTE SENSING AND VALIDATION OF SURFACE CURRENTS FROM HF RADAR

by

Darryl C. Melton

September, 1995

Thesis Advisor: Jeffrey D. Paduan

Approved for public release; distribution is unlimited.

REPORT DOCUMENTATION PAGE	Form Approved OMB No. 0704-

1. AGENCY USE ONLY *(Leave blank)*	2. REPORT DATE September 1995	3.REPORT TYPE AND DATES COVERED Master's Thesis

4. TITLE AND SUBTITLE Remote Sensing and Validation of Surface Currents From HF Radar	5. FUNDING NUMBERS
6. AUTHOR(S) Darryl C. Melton	
7. PERFORMING ORGANIZATION NAME(S) AND ADDRESS(ES) Naval Postgraduate School Monterey CA 93943-5000	8. PERFORMING ORGANIZATION REPORT NUMBER
9. SPONSORING/MONITORING AGENCY NAME(S) AND ADDRESS(ES)	10. SPONSORING/MONITORING AGENCY REPORT NUMBER

11. SUPPLEMENTARY NOTES The views expressed in this thesis are those of the author and do not reflect the official policy or position of the Department of Defense or the U.S. Government.

12a. DISTRIBUTION/AVAILABILITY STATEMENT Approved for public release; distribution is unlimited.	12b. DISTRIBUTION CODE

13. ABSTRACT *(maximum 200 words)*

Radial current data from the CODAR HF radar network around Monterey Bay, California, were analyzed for the period of August-December 1994. Previous studies in Monterey Bay used total vector current data. Long-term percent coverage maps showed that coverage decreased radially, vice range, from the site. Through statistical examination of radial current data from the Santa Cruz and Point Piños SeaSonde sites and the Moss Landing CODAR site, comparisons along and around the baseline between systems were used to assess system performance. Significant discrepancies were discovered in the directional information from the Point Piños and Moss Landing sites. Point Piños' error was approximately 10° counterclockwise and Moss Landing's error was approximately 5° counterclockwise. RMS differences among even the best correlated baseline pairs were approximately 15 cm/s. Data from the baseline was used to select vector currents when the baseline difference was less than 10 cm/s for comparisons with independent nearby moored current observations. This subsampled data did not show significantly better correlation with the moored data than the full data set. Analysis of the radial error estimates provided by the system algorithms determined that no correlation exists between absolute value difference of the radial velocities along the baselines between systems and these built in error estimates.

14. SUBJECT TERMS: CODAR, SeaSonde, HF Radar, Surface Currents	15. NUMBER OF PAGES 77
	16. PRICE CODE

17. SECURITY CLASSIFICATION OF REPORT	18. SECURITY CLASSIFICATION OF THIS PAGE	19. SECURITY CLASSIFICATION OF ABSTRACT	20. LIMITATION OF ABSTRACT
Unclassified	Unclassified	Unclassified	UL

NSN 7540-01-280-5500

Standard Form 298 (Rev. 2-89)
Prescribed by ANSI Std. 239-18 298-102

Approved for public release; distribution is unlimited.

REMOTE SENSING AND VALIDATION OF SURFACE CURRENTS FROM HF RADAR

Darryl C. Melton

Lieutenant, United States Navy
B.S., United States Naval Academy, 1988

Submitted in partial fulfillment
of the requirements for the degree of

MASTER OF SCIENCE IN METEOROLOGY AND PHYSICAL OCEANOGRAPHY

from the

NAVAL POSTGRADUATE SCHOOL
September 1995

Author: [redacted]
Darryl C. Melton

Approved by: [redacted]
Jeffrey D. Paduan, Thesis Advisor

[redacted]
Newell Garfield, Second Reader

[redacted]
Robert H. Bourke, Chairman
Department of Oceanography

ABSTRACT

Radial current data from the CODAR HF radar network around Monterey Bay, California, were analyzed for the period of August-December 1994. Previous studies in Monterey Bay used total vector current data. Long-term percent coverage maps showed that coverage decreased radially, vice range, from the site. Through statistical examination of radial current data from the Santa Cruz and Point Piños SeaSonde sites and the Moss Landing CODAR site, comparisons along and around the baseline between systems were used to assess system performance. Significant discrepancies were discovered in the directional information from the Point Piños and Moss Landing sites. Point Piños' error was approximately 10° counterclockwise and Moss Landing's error was approximately 5° counterclockwise. RMS differences among even the best correlated baseline pairs were approximately 15 cm/s. Data from the baseline was used to select vector currents when the baseline difference was less than 10 cm/s for comparisons with independent nearby moored current observations. This subsampled data did not show significantly better correlation with the moored data than the full data set. Analysis of the radial error estimates provided by the system algorithms determined that no correlation exists between absolute value difference of the radial velocities along the baselines between systems and these built in error estimates.

TABLE OF CONTENTS

I. INTRODUCTION 1
A. HF RADAR 2
B. USES FOR HF RADAR 2
C. CODAR 4
1. How CODAR Works 4
2. CODAR Deployment Around Monterey Bay . . . 5
3. Recent Results from Studies in Monterey Bay 6
D. SOURCES OF ERROR TO CODAR MEASUREMENTS 8

II. DATA AND METHODS 17
A. LONG TERM RADIAL CURRENT COVERAGE PATTERNS . . . 18
1. Santa Cruz Radial Current Coverage Pattern 19
2. Point Piños Radial Current Coverage Pattern 19
3. Moss Landing Radial Current Coverage Patterns 20
B. BASELINE ANALYSIS 21
1. Point Piños-Santa Cruz Baseline 23
2. Moss Landing-Santa Cruz Baseline 24
3. Point Piños-Moss Landing Baseline 24
4. Results from Baseline Comparisons 25
C. TIME SERIES BASELINE ANALYSIS 26
1. Results from Standard Baseline Gridpoints . 26
2. Comparison with Moored Current Observations 27
D. RADIAL ERROR ESTIMATE ANALYSIS 28
1. Histogram Plots 29
2. Scatter Plots 29

III. SUMMARY 53

A. CORRELATION AND RMS DIFFERENCE ANALYSIS 53
B. TIME SERIES OF BASELINE PAIRS 55
C. RADIAL ERROR ESTIMATE ANALYSIS 56
D. RECOMMENDATIONS 57

LIST OF REFERENCES 63

INITIAL DISTRIBUTION LIST 65

ACKNOWLEDGEMENT

I wish to thank Dr. Jeff Paduan for his guidance, expertise, and patience during this thesis. Without his assistance, this task would have been much more stressful.

I would also like to extend a most hearty thanks to Mr. Mike Cook of the Naval Postgraduate School Oceanography Department for his expert computer programming and assistance. His assistance has helped this computer illiterate graduate school student become functionally literate.

I. INTRODUCTION

With the end to the cold war, the United States Navy's focus has shifted from a blue water, global conflict, scenario to a littoral, regional conflict scenario. This has resulted in a greater need to understand the oceanographic processes present in the littoral zone. Advances in satellite imagery instruments and techniques have contributed to this need. For example, imagery from the Advanced High Resolution Radiometer (AVHRR) sensor has proven useful in identifying significant large scale features and the basic flow structures associated with them. However, this sensor and some other satellite sensors are severely limited by the presence of clouds. They also provide only indirect measurements of surface currents. Therefore, a true need exists for a reliable system which will be less affected by weather and which can provide direct current observations. In recent years, radars operating in the high frequency (HF) band (3-30 MHz) have been developed that measure surface currents and tides remotely.

One particular type of HF radar system is currently in use around the Monterey Bay. A network of Coastal Ocean Dynamics Applications Radar (CODAR) systems measure radial current velocities that, when combined, provide maps of vector currents. In this thesis, I take a step backwards in studying the CODAR system. Previous studies utilized the total current vector maps produced by the network in order to describe surface currents and tidal influences seen in Monterey Bay. However, I use the raw radial current data provided from each site for the period of 01 August to 31 December 1994 to help establish the accuracy of total current vector maps which are produced from them. Until now, this has not been done.

A. HF RADAR

Nearly forty years ago, the first study using HF radar for oceanographic purposes revealed that the echoes scattered from the ocean surface contain a Doppler frequency shift which is directly related to the motion of incoming or departing wave trains of a particular wavelength. Crombie (1955) discovered that the peak return signal from the radiated energy results from first-order Bragg scattering off surface gravity waves whose wavelength is equal to one-half the transmitted wavelength. The resulting signal, therefore, provides the velocity directly toward or away (radially) from the individual radar antenna by measuring the Doppler shift of the returned energy due to the (known) motion of reflecting waves plus the motion of the underlying water. Figure (1) (Barrick et al., 1977) illustrates the Bragg scatter effect and the types of Doppler shifts expected from advancing and receding waves. Stewart and Joy (1974) qualitatively demonstrated the accuracy of deriving the surface current radial velocities from HF radar returns. The frequency of the radar also affects the depths at which the currents are "sensed". The average depth sensed by the radar is approximately the radar wavelength, λ, divided by 8π (Stewart and Joy, 1974), which is on the order of one meter for the frequencies in use.

B. USES FOR HF RADAR

In oceanography, many uses for HF radar exist. By establishing a historical data base of surface currents in Monterey Bay, long term effects of many oceanographic processes can be studied. Larval transport and pollution tracking are just two of the many areas of study possible.

With the recent flood on the Monterey Peninsula in March 1995, CODAR could have been effective in establishing the magnitude and direction of surface currents which were present to transport the fertilizers and other contaminants which flowed into the bay from the vast farming areas washed out by the flood waters. Other possible uses include: search and rescue missions, assistance for local fishing efforts, marine biological research, among others.

Along with the many civilian uses, many military uses of the HF radar systems exist. With the transition from a blue water conflict to the littoral conflict strategy, the need for accurate measurements of coastal oceanographic processes has risen to the forefront. To achieve a success in the shallow water environment, an accurate depiction of the surface and tidal currents must be known. However, in time of war, typical in situ instruments deployed from oceanographic research and survey ships will not meet the need. Therefore, the need exists for an accurate remote sensing system which can be quickly and safely deployed which will yield the required data in real-time. The CODAR system is just such a system.

With HF radar, true measurements of surface currents could be determined in a relatively short amount of time, whereas, techniques used from AVHRR imaging to depict small scale processes is less accurate and more weather limited. Amphibious assault landings could be better planned when an HF radar system is in place. If data can be collected for a time period of two to four weeks in advance of a proposed landing, tidal and coastal currents could be predicted into the future to better plan for landing operations. Mine drift predictions could be more accurately made, thus enhancing the effectiveness of proposed mine fields or fine tuning of mine hunting procedures and tactics. HF radar systems could also be placed in strategic locations to provide safer navigation

through restricted channels and waterways approaching harbors and roadsteads where U.S. Navy vessels are moored or anchored, which would provide real-time tide and current information vice a total reliance on tide and current tables and calculations.

C. CODAR

Since the development of CODAR at the National Oceanic and Atmospheric Administration's (NOAA) Wave Propagation Laboratories in the early 1980's, the system has been deployed in numerous regions for a variety of uses. Here in the Monterey Bay, a unique situation exists with the manner in which the network of CODAR systems is deployed. For the first time, a network of three systems has been operated around a bay in which all three baselines exist over water. A baseline is the line between two radar systems. This provides the unique opportunity to evaluate the accuracy of the system by comparing radial current velocities for the same parcel of water obtained from two different radar sites.

1. How CODAR Works

A high frequency pulse is transmitted from the CODAR antenna and the return signal, at multiple frequencies, is processed to determine radial current speed and direction. The manner in which this is done is related to antenna design and the associated software of the CODAR system. A pair of orthogonally mounted cross looped antennas are mounted on a single monopole antenna. An HF signal is transmitted omnidirectionally from the monopole antenna. Distance from the antenna site is easily determined from the time delay of the return signal from the transmitted pulse (range gating). The pointing method used to determine bearing from the antenna site is, however, considerably more complicated. CODAR

systems employ direction finding techniques. Because each of the three antenna elements (one monopole and two cross looped) has a different, and known, beam pattern as a function of look angle, the ratio of antenna strengths indicates the direction from which the signals originated (Lipa and Barrick, 1983).

The older CODAR system collects backscattered data over a 30-minute period and requires about 90 minutes to process the results, whereas, the SeaSonde systems collect backscattered data continuously and compute radial currents based on a running average over 60 minutes (Paduan and Rosenfeld, 1995). Data from two or more sites within a circular region of 3 km radius are combined to produce a total current vector map. Figures (2) through (4) are examples of radial current maps produced from the five month data set used in this study. Each is a five month average of radial current velocities where radial current vectors shown were comprised from radial bins which had a greater than five percent coverage for the five month period. Figure (5) is a total current vector map produced from the least squares combination method of Lipa and Barrick (1983) using radial currents from each the three sites around Monterey Bay. In this figure, vector currents are shown only for locations that had vector estimates at least 50% of the time.

2. CODAR Deployment Around Monterey Bay

Three CODAR sites were in operation around Monterey Bay during this study. Those sites form a network that provides nearly complete coverage of the bay every two hours. Two of the three sites are the newer generation SeaSonde systems, which are an improved version of the original CODAR system. The important differences include: Frequency Modulated Continuous Wave (FMCW) transmit technology instead of pulsed transmissions, (the greater efficiency of this method means the average power consumption is 100 W rather than 1 KW), lower frequency (11.5-13.5 MHz vs. 25.4 MHz for

the original CODAR), higher sampling rates (weighted average over 1 hour versus a 30 minute sample every 2 hours for the original CODAR), and very much more compact antennas. SeaSondes provide a higher sampling rate than the older CODAR system since they are continuously sampling and can provide hourly current observations, whereas, the CODAR system only samples for 30 minutes during each 2 hour time period. The SeaSonde sites are located at the Long Marine Laboratory in Santa Cruz, California, and at Point Piños in Pacific Grove, California. The original CODAR site at the Monterey Bay Aquarium Research Institute, Moss Landing, California, operates at the higher 25.4 MHz frequency. Hence, its coverage range is significantly lower. Figure (6) (Paduan and Rosenfeld, 1995) illustrates the positions of the three CODAR systems used in this study together with the decommissioned CODAR site at Hopkins Marine Station in Pacific Grove, CA, and the SeaSonde site at Granite Canyon, south of Monterey Bay. The coverage arcs shown are representative of the ranges of the respective systems.

3. Recent Results from Studies in Monterey Bay

Recent studies conducted around Monterey Bay utilized total current vector data provided by the manufacturer under contract to NOAA and the Office of Naval Research. Data from the two-site CODAR network collected in 1992 was analyzed for its view of surface currents within Monterey Bay at periods from tidal to monthly. Neal (1992) described the monthly averaged circulation patterns for the spring period. He found variable long-term averages in March and April but a persistent cyclonic circulation pattern in May that was centered northwest of Moss Landing with strongest monthly averaged currents (~20 cm/s) in the outer, southward flowing portion of the pattern. He also investigated the diurnal variations of surface currents in Monterey Bay by computing the canonical day for the March-May period, which

was done by averaging all total current vector maps at common times. The typical daily pattern revealed a strong influence of the diurnal sea breeze forcing. Currents were strongest in the late afternoon and aligned toward the southeast direction of the Salinas Valley and the sea breeze winds. Currents were weak or offshore at night.

Foster (1993) also investigated the diurnal variation of surface currents from the two-site CODAR network using data from September 1992. He confirmed the canonical day variations seen in the spring data and showed how the complete daily cycle includes strong flow toward shore and the Salinas Valley for a short period in the late afternoon followed by clockwise rotation of the surface current that actually precedes the weakening of the sea breeze winds. Petruncio (1993) used this same data to describe surface tidal currents in the Monterey Bay. Diurnal fluctuations as reflected by the K1 tidal constituent were shown to be dominated by the sea breeze-driven diurnal fluctuations in the near-surface CODAR data. Ellipses were uniformly aligned with the axis of the Salinas Valley and the amplitudes (~25 cm/s) were very large compared with diurnal fluctuations measured at the M1 mooring just 17 m below the surface of ~3 cm/s. At the semi-diurnal frequency (M2 tidal constituent), amplitudes of the fluctuations in the CODAR-derived currents were similar to those from the mooring. Furthermore, the spatial pattern of semi-diurnal tidal ellipses from the CODAR data showed obvious alignment with topography: amplitudes were largest over the head of the Monterey Submarine Canyon and semi-major axes were aligned with the continental shelf, which supports the hypothesis of a growing and breaking internal tidal wave traveling up from the canyon (Broenkow and Smethie, 1978).

Data from the three-site CODAR/SeaSonde network for 1994 has also been analyzed using the total current vector data produced by the manufacturer (Paduan et al., 1995; Paduan

and Rosenfeld, 1995). In the summer months, the mean cyclonic pattern is similar to what was found in the CODAR data from the spring and summer of 1992, although the magnitudes in the mean pattern are consistently stronger than was observed in the 1992 data. At the mouth of the Monterey Bay, a strong alongshore flow is observed with evidence of a second eddy circulation pattern in the outer parts of the radar domain. The data from October-December 1994 showed more variable currents with monthly averaged northward flow along the outer portion of Monterey Bay showing up in the December results.

Paduan and Rosenfeld (1995) conducted extensive comparisons with long time series observations from the M1 mooring. Radar-derived currents were compared with moored Acoustic Doppler Current Profiler (ADCP) current observations from 10 m depth. Low-passed-filtered time series were highly correlated with a complex correlation magnitude of 0.79 and phase near zero. The times of largest disagreement were related most strongly to large wind stress events. There was a significant complex correlation between the HF-ADCP velocity difference and wind stress of magnitude 0.50. (Similar attempts to correlate velocity differences with near-surface temperature stratification showed low correlation.) Direct correlation of radar-derived currents and wind stress was also very high (magnitude 0.57) and the average direction difference (surface current 48.5° to the right of wind stress) was consistent with predictions from Eckman theory.

D. SOURCES OF ERROR TO CODAR MEASUREMENTS

Two factors determine the accuracy of CODAR (and almost every remote sensing device): noise and system resolution (Barrick et al., 1985). Reduction of accuracy can occur if the signal peaks of the measured signal are difficult to

distinguish from the background noise. Through the use of averaging techniques, some of the uncertainty in the surface current fields can be removed. Conversely, drawbacks occur when too much averaging is conducted because the resolution of smaller scale features is reduced.

CODAR system antennas are also susceptible to electromagnetic interference from surrounding metallic structures which can induce error into the data fields. This occurs because the CODAR direction finding algorithm assumes a beam pattern for each of the three antenna elements based on theoretical or laboratory-determined patterns. If the actual beam patterns on site differ from the assumed patterns, pointing errors may result. For example. Figure (7) illustrates the power patterns for the crossed-loop elements during a particular laboratory experiment compared to the theoretical cosine-squared prediction (Lipa and Barrick, 1983).

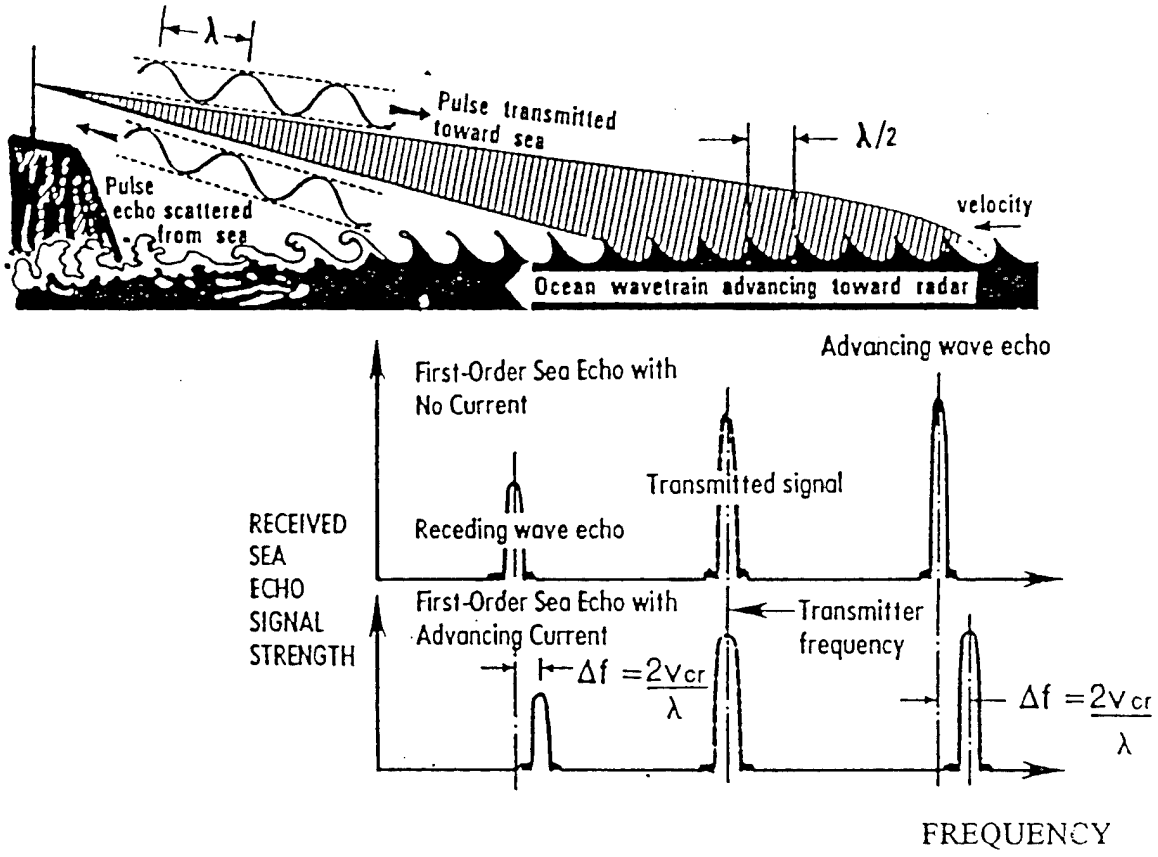

Figure 1. Illustration of the first-order Bragg scattering effect of an HF radar pulse incident on the sea surface and the associated Doppler shifts from surface gravity waves with and without an underlying current (Barrick et al., 1977).

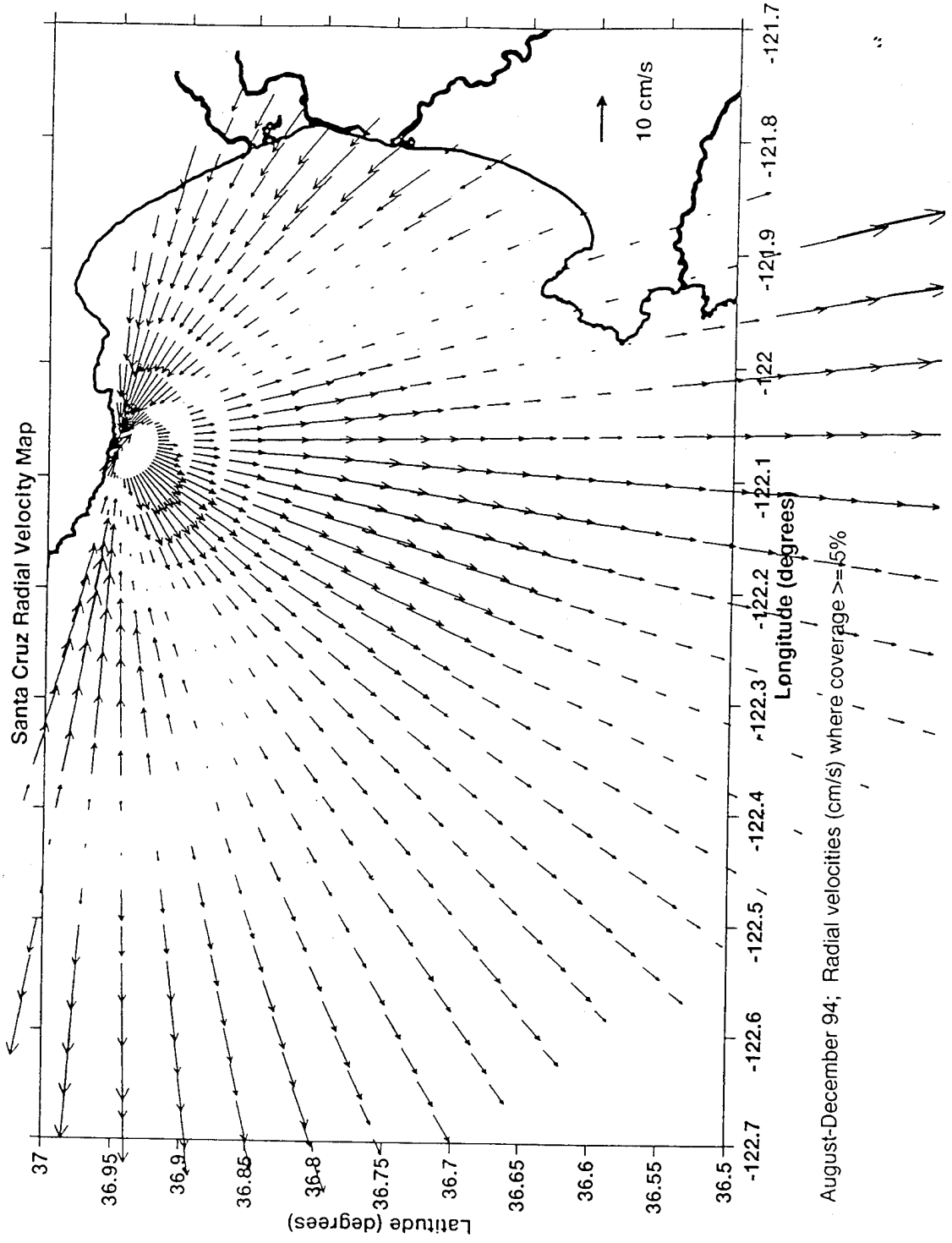

Figure 2. Mean radial current map for the Santa Cruz SeaSonde site for the period of August through December 1994.

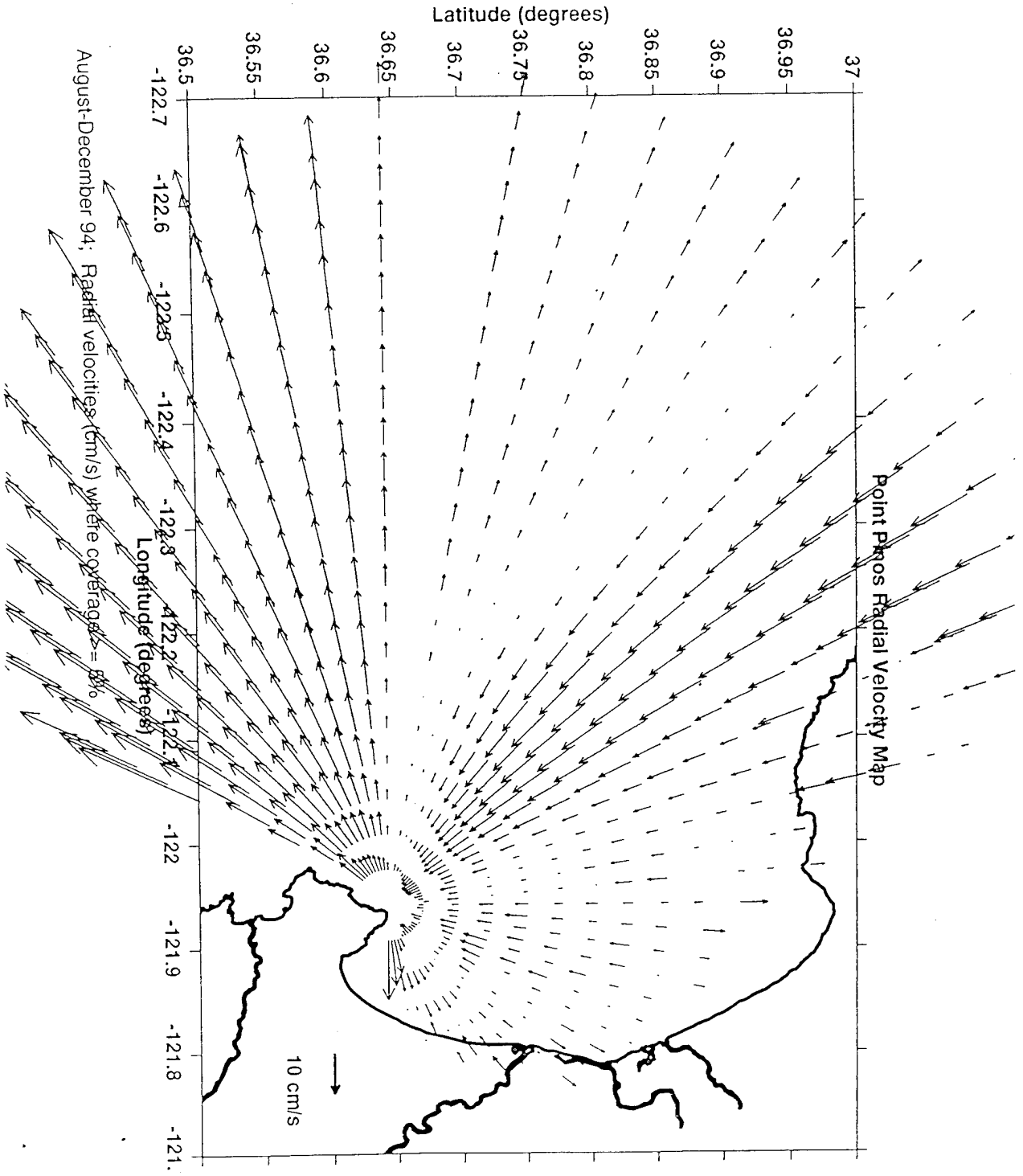

Figure 3. Mean radial current map for the Point Piños SeaSonde site for the period of August through December 1994.

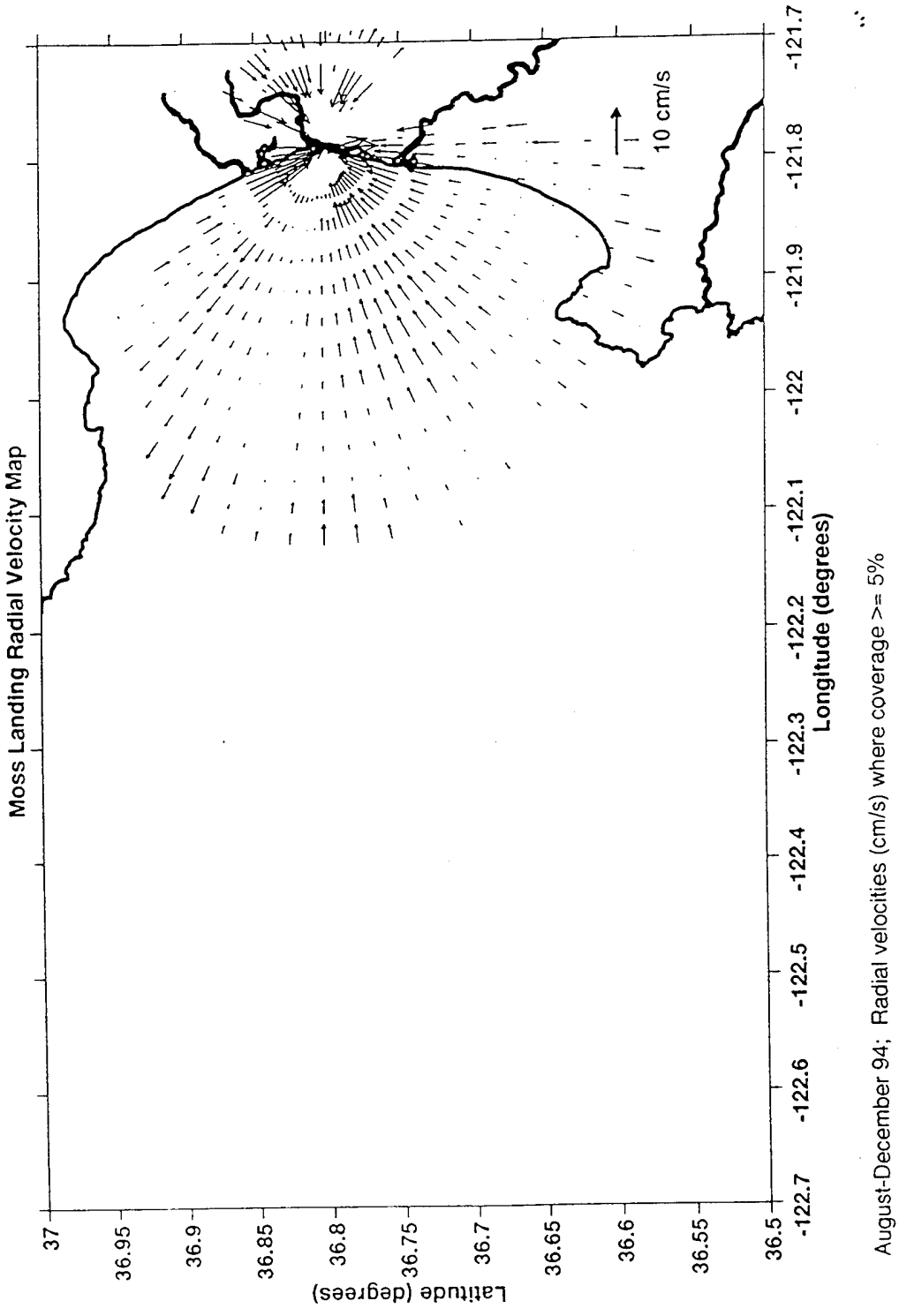

Figure 4. Mean radial current map for the Moss Landing CODAR site for the period of August through December 1994.

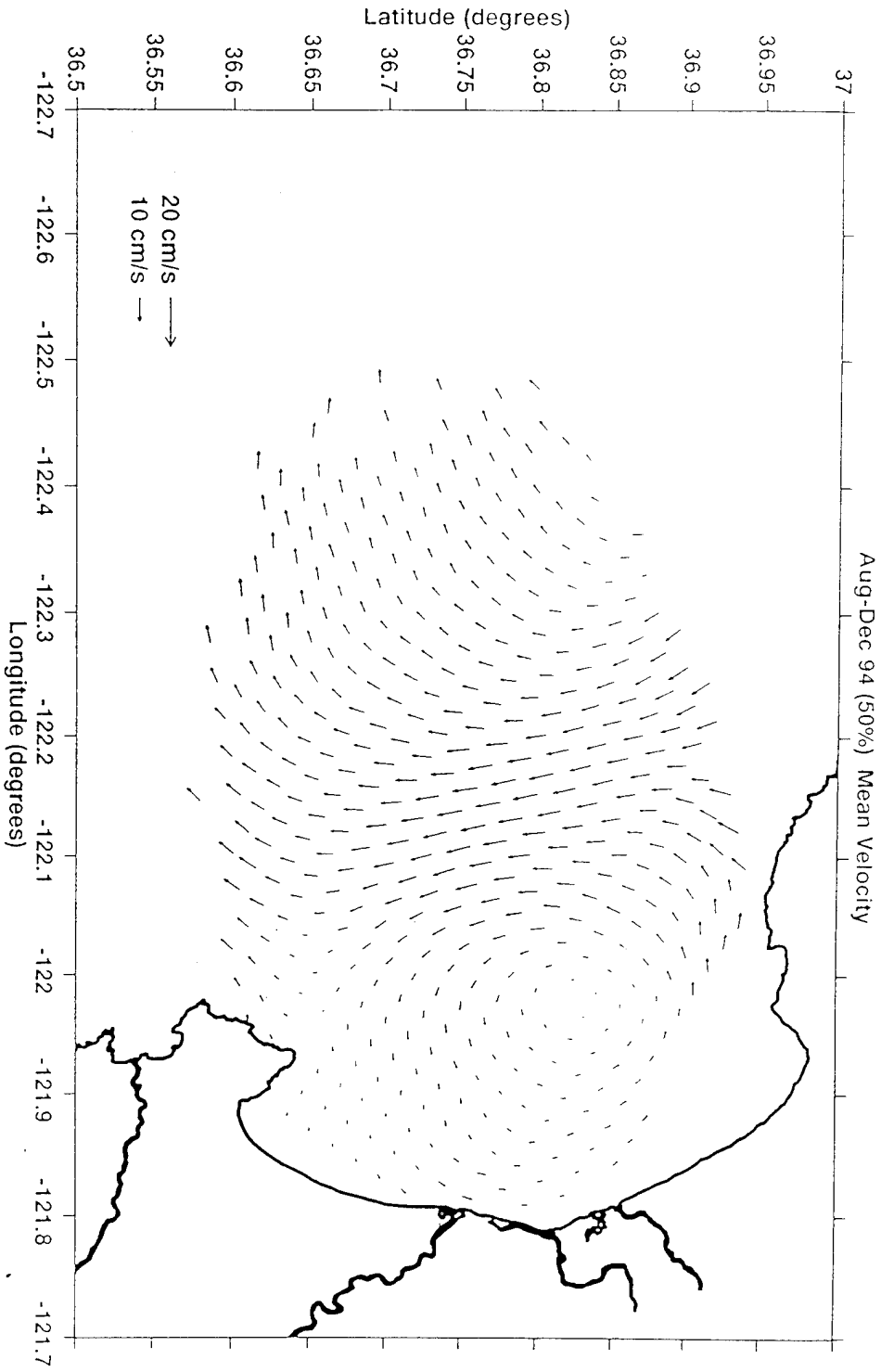

Figure 5. Total mean current velocity map for the period of August through December 1994 based on radial data from each of the three sites around Monterey Bay. Total current vectors from radial bins less than 50% coverage are not shown in this map.

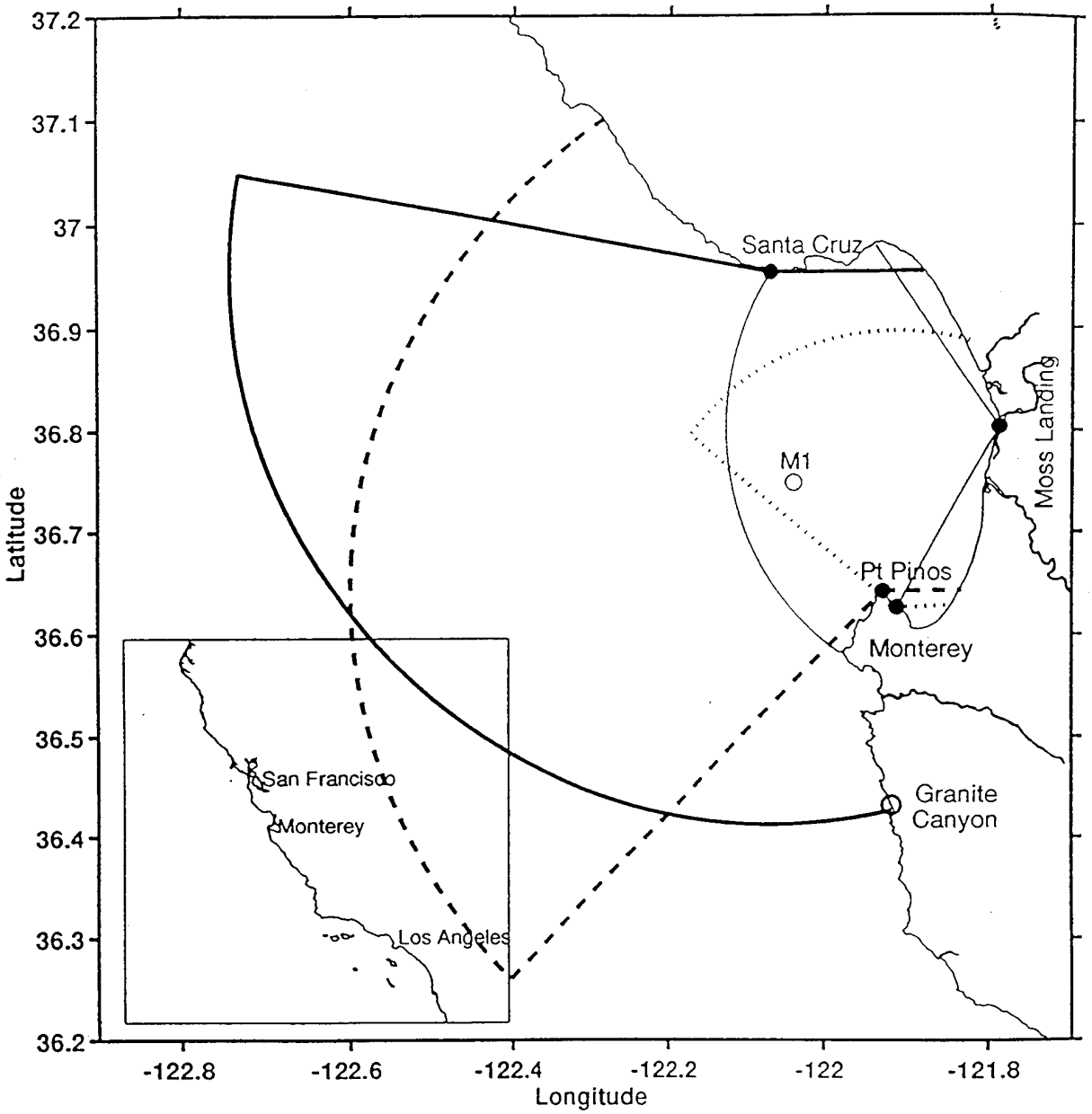

Figure 6. SeaSonde/CODAR antenna locations around Monterey Bay. The arcs shown denote the nominal range of each radar system. The heavy solid line represents the SeaSonde coverage from Santa Cruz and the heavy dashed line represents the SeaSonde coverage from Point Piños. The light solid line represents Moss Landing's CODAR coverage. The remaining light dashed line represents the coverage from the CODAR system at Hopkins Marine Laboratory, which is no longer in use, and the symbol labeled M1 denotes the location of moored ADCP observations.

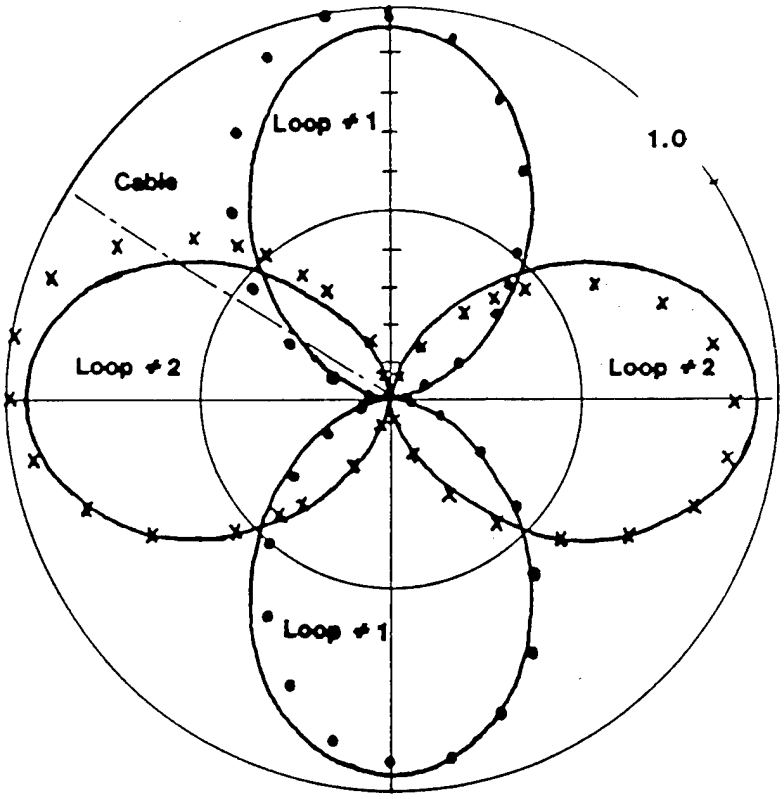

Figure 7. Power patterns for the crossed-loops measured on a turntable (dots and crosses) compared to the theoretical cosine-squared prediction; scale is linear in normalized power , with circles at 1.0 and 0.5 (Lipa and Barrick, 1983).

II. DATA AND METHODS

In conducting this study, I was afforded the opportunity to examine the output from CODAR-type HF radar systems in a unique way. In few other published reports has a study been conducted in which network baselines existed over water. Previous deployments of CODAR either were deployed along a straight coastline where the baselines existed over land or the radial current data that were used to produce total current vector maps were not examined. (An exception includes the results reported by Essen et al. (1989) based on deployment of two CODAR systems in the Norwegian Channel. During an 11-day period, they obtained agreement between the two systems that exceeds that reported below based on a 5-month period.) With the network around Monterey Bay, three baselines exist over water, which is a unique configuration.

Various statistical means were used to validate surface currents determined from the CODAR system. Five month coverage patterns were generated showing the percentage of time observations were obtained at each radial bin for each of the three sites used in the study. Baseline comparisons were exploited in several ways. After standard baseline gridpoints were determined, correlations were conducted to check how well data from each site compared and to evaluate whether better correlated pairings existed away from the geographic baseline. Root mean square (RMS) differences between the same standard gridpoint pairings and best correlated pairings were then taken to determine how high the respective differences were and if they could be attributed to resident noise in the system. From these correlations and RMS differences, inferences about pointing errors were made. Comparisons were also made for the standard baseline gridpoint between Santa Cruz and Point Piños and the M1 mooring to establish whether baseline comparison levels were related to the agreement

between CODAR-derived vector currents and independent moored current observations. Finally, the radial error estimates provided in the system files were checked against baseline comparison levels in order to determine their usefulness as weighting factors in the total vector mapping process.

A. LONG TERM RADIAL CURRENT COVERAGE PATTERNS

The direction finding algorithm used by CODAR-type HF radar systems does not provide observations at every angle bin for a given range at every time. The number of angle bins observed depends on the physical range of current speeds encountered over the range cell because this current range determines the width of the Bragg peak in the backscattered observations. It is expected that the particular angle bins observed would move around with time and that the overall coverage would decrease with range due to signal-to-noise limitations. If these expectations were borne out, average coverage patterns would be a function of range only and not direction. Figures (8) through (10) are coverage maps produced from the five months of data used in this study. These coverage maps, each annotating coverage from one of the three system sites, reveal some disturbing information about the antenna radiation patterns. One would expect that the percent coverage would decrease as the distance from the respective sites increased. This is, however, not what is seen. For each site, the coverage did not decrease appreciably as a function of distance (until the maximum ranges were reached), but more so as a function of angle. One conclusion from these findings could be that the antenna patterns are distorted such that the direction finding algorithms under sampled some angles and over sampled others.

1. Santa Cruz Radial Current Coverage Pattern

Figure (8) is the five month radial current coverage pattern for the Santa Cruz SeaSonde site. The pattern is not what we would expect to see. Here the percent coverages fall off radially in each direction from an angle of 256° from the site (measured counterclockwise from east). The center portion of the pattern has a relatively low coverage percentage (between 40-49%) up to a range of approximately 18 km. Just to the east and west of this low range area, the percentage of coverage increases to over 50% before falling off to less than 10% on the far eastern and western extremes of the Santa Cruz coverage. Another unique characteristic of this pattern is that, near the center of the pattern, the percent coverages increase to over 70% as the range from the site increases to approximately 36 km. A possible explanation for this increase in coverage could be the predominant winds from the northwest entering the Monterey Bay region, however, further study is required to ascertain whether this is truly a factor, as opposed to antenna pattern distortion.

2. Point Piños Radial Current Coverage Pattern

Figure (9) is the five month radial current coverage pattern for the Point Piños SeaSonde site. As discussed above, this pattern is also contrary to the decreasing coverage with range pattern that we would expect to see. The coverage percentages fall of radially away from the center of the coverage pattern, which is approximately 155° from the site (measured counterclockwise from east). Highest coverage percentages in this pattern are aligned to the northwest which could be related to the primary wind/wave direction. The coverage percentages for the Point Piños site are consistently higher than those seen in the Santa Cruz pattern. These higher percentages over Santa Cruz may be related to the winds and waves approaching the Point Piños site, whereas, the winds and waves pass obliquely to the Santa Cruz site.

One of the striking properties of this pattern is the missing data seen in the 175° radial from the Point Piños site (measured counterclockwise from east). This missing radial is seen in all three of the systems. However, Point Piños is the only one to have this missing radial over water and in the field of view. The lack of data along this radial is indicative of a problem in the processing algorithm and not the antenna system itself. This discovery was made for the first time in this study, since this was the first time radial coverage maps were produced for each site in the Monterey Bay CODAR network vice total coverage pattern maps from the combination of the three sites.

3. Moss Landing Radial Current Coverage Patterns

Figure (10) is the five month radial current coverage pattern for the Moss Landing CODAR site. As seen in the patterns from Santa Cruz and Point Piños, the percent coverage decreases radially from the radial angle of 165.2° (measured counterclockwise from east). Similar to the Point Piños site, the highest percent coverage (70-79%) area appears to be aligned toward the northwest, the direction of the predominant winds and waves. Coverage ranges are significantly lower for the Moss Landing system than for the other systems due to the higher frequency of transmission used, transmitter design, etc., but the percentages of coverage are higher than those seen for the Santa Cruz system. As mentioned earlier, this appears to be a function of antenna location and look angle with respect to the wind/wave direction. However, further study is required to confirm this hypothesis. Unlike the patterns from the other sites, the Moss Landing coverage pattern includes a significant amount of data over land. This is possibly a function of the older CODAR system, but it is indicative of some antenna pattern distortion and interference problems.

B. BASELINE ANALYSIS

Since three baselines exist over water in the Monterey Bay CODAR network, a true measure of system performance could be gained by examining radial current data provided by two different sites along a given baseline. In theory, at any given baseline gridpoint pairing, both sites along that baseline should provide the same magnitude for the radial current present. Since one site would indicate that the given current was approaching and the opposite site along the baseline would indicate that the given current was receding, the opposite sign is expected.

In order to analyze the respective baselines, the radial bin distribution was necessary to establish the baseline positions. Figure (11) illustrates the relative positions of radial bins from each of the three sites overlaid on the same geographical plot. The newer SeaSonde bins are located at increasing 3 km incremental ranges and 5° azimuthal spacing from the Santa Cruz and Point Piños sites, whereas, the CODAR bins are located at increasing 2.4 km incremental ranges and 5° azimuthal spacing from the Moss Landing site. Once these relative positions were known, the baselines were overlaid to determine the best baseline gridpoint pairings to examine. The baselines were determined from geometry obtained from the latitude and longitude positions of each of the CODAR/SeaSonde sites. These pairings are annotated in Figure (12). This figure shows only radial bins near the respective baselines and highlights the particular bins selected for scrutiny in this study. Table (1) lists the range and direction of these standard baseline gridpoint pairings used to conduct the subsequent correlation and RMS difference analyses.

Once the gridpoint pairings were established, correlation and RMS difference analyses were conducted by holding one gridpoint (radial bin) constant and comparing it to all of the

respective radial bins emanating from the *opposite* site along the baseline at the given gridpoint range. For example, along the Santa Cruz-Point Piños baseline, all 18 km radial bins emanating from Santa Cruz were compared with all 18 km radial bins emanating from Point Piños.

Baseline	Angle (1)	Range (1)	Angle (2)	Range (2)
SCruz(1)-Pt. Piños(2)	286°	18 km	110°	18 km
SCruz(1)-M. Landing(2)	326°	18 km	150.2°	11.1 km
Pt. Piños(1)-M. Landing(2)	055°	12 km	230.2°	11.1 km

Table 1. Standard baseline gridpoint pairings with angles (referenced to east) and range from the radar sites. Numbers in parenthesis represent the specific site from which the data is referenced.

This process is depicted graphically in Figure (13) for the case of a Santa Cruz-Pt. Piños baseline pair. This process was repeated for each of the standard baseline pairs in Table 1 from each direction yielding six sets of data.

Before correlations or RMS differences could be computed between pairs of radial current time series, it was necessary to select out only those times when an observation was present from both radar sites. An example of unprocessed time series is presented in Figure (14), which shows the radial current time series from the two standard baseline gridpoints along the Santa Cruz-Pt. Piños baseline highlighted in Figure 12 and Table 1. It is clear from those unprocessed time series that the baseline currents do not agree within the nominal 4 cm/s resolution of the instruments. The RMS differences and time series plots of the matched points in the next sections quantify this impression.

1. Point Piños-Santa Cruz Baseline

Along the Point Piños-Santa Cruz baseline the predicted result would be that the standard baseline pairing of 110°/18 km from Point Piños and 286°/18 km from Santa Cruz would have the highest correlation and the lowest RMS difference (all angles measured from each site are referenced to east). However, the data clearly show that this was not the case. After correlations and RMS differences were taken for all 18 km radial bins emanating from both sites, the results were plotted as a function of angle. Figures (15) and (16) graphically illustrate these results. In these figures, the standard baseline gridpoint which is being compared to all radial bins from the opposite site is shown by the solid curve and the best correlated radial bin (determined from the correlation matrix of all 18 km radial bins from one site compared to all 18 km radial bins from the opposite site) is shown by the dashed curve. The solid vertical line indicates the angle of the baseline gridpoint from the opposite site (the intersection of the solid vertical line and the solid curve represents where the peak in correlation and the lowest point in RMS difference is *expected* to occur).

The standard baseline gridpoint from Santa Cruz had the highest correlation and lowest RMS difference, hence, in Figure (15) there is only one curve represented since the standard baseline gridpoint curve and the best correlated curve are one in the same. The Santa Cruz SeaSonde site, therefore, does not exhibit pointing errors based on this 1994 data set. The dropout in the RMS difference curve at 175° in the figure is due to the missing data sector from the Point Piños site. The highest correlated radial bin from Point Piños with the Santa Cruz baseline gridpoint was at 120°/18 km from Point Piños (Figure 16). Thus, a ten degree discrepancy existed from the Point Piños site.

2. Moss Landing-Santa Cruz Baseline

For the Moss Landing-Santa Cruz baseline, the expected highest correlated and lowest RMS difference pairing would be the standard baseline gridpoint pairs of 150.2°/11.1 km from Moss Landing and 326°/18 km from Santa Cruz. Figures (17) and (18) graphically illustrate these results which show that the standard gridpoint pairs do not have the highest correlation or lowest RMS difference. As stated above, the standard baseline gridpoint which is being compared to all radial bins at that standard gridpoint range from the opposite site is shown by the solid curve and the best correlated radial bin is shown by the dashed curve. The solid vertical line indicates the angle of the baseline gridpoint from the opposite site. The intersection of the solid line and the vertical line denotes the pairing which should have yielded the highest correlation and the lowest RMS difference. After correlations and RMS differences were taken for all radial bins emanating from both sites, the standard baseline gridpoint from Santa Cruz again had the highest correlation and lowest RMS difference, indicating that the system is not exhibiting pointing errors. The highest correlated radial bin from Moss Landing with the Santa Cruz baseline gridpoint was at 155.2°/11.1 km from Moss Landing. Thus, a five degree discrepancy existed from the Moss Landing site.

3. Point Piños-Moss Landing Baseline

The predicted result for the Point Piños-Moss Landing baseline, would be that the standard baseline pairing of 055°/12 km from Point Piños and 230.2°/11.1 km from Moss Landing would have the highest correlation and the lowest RMS difference. Figures (19) and (20) graphically illustrate that the expected results were not achieved. As shown in earlier figures, the baseline gridpoint which is being compared is shown by the solid curve and the best correlated radial bin is shown by the dashed curve. The intersection of the solid vertical line and the solid curve represents where the peak in

correlation and the lowest point in RMS difference should have occurred. The highest correlated radial bin from Point Piños with the Moss Landing baseline gridpoint was at 060°/12 km from Point Piños. A five degree discrepancy, therefore, existed from the Point Piños site. The highest correlated radial bin from Moss Landing with the Point Piños baseline gridpoint was at 245.2°/11.1 km from Moss Landing. Thus, a fifteen degree discrepancy existed from the Moss Landing site. The dropout in the RMS difference curve at 175° in Figure (20) is due to the missing data sector from the Point Piños site.

4. Results from Baseline Comparisons

The resulting discrepancies found at the respective network sites is conclusive that a pointing error exists in two of the three CODAR/SeaSonde sites. The pointing errors found in this study are likely attributable to antenna problems and the complexity of the pointing methods used in the system software. Assuming that Santa Cruz has the best alignment gives the most consistent results for the three-site network. To correct for the discrepancies in the other two sites, the Point Piños radial data field should be rotated ten degrees clockwise and the Moss Landing radial field should be rotated five degrees clockwise. The resulting radial fields would bring the Santa Cruz-Point Piños and the Santa Cruz-Moss Landing baselines back into proper alignment. Along the remaining baseline (Point Piños-Moss Landing), the shift would bring the best correlated and lowest RMS difference pairs within five degrees of each other. Given that the radial bins are more closely spaced along the shorter ranges from the Moss Landing system, this would seem to be acceptable. However, the resulting Moss Landing baseline has a suspicious orientation: the new alignment would appear to have the new baseline oriented between the Moss Landing site and the old CODAR site located at the Hopkins Marine Laboratory in Pacific Grove, California. RMS differences values for the standard

baseline gridpoints and the best correlated gridpoints provide an overall measure of system performance. Results are summarized in Table 2. For the best correlated pairs, RMS differences over that five month period range from 15-17 cm/s.

C. TIME SERIES BASELINE ANALYSIS

1. Results from Standard Baseline Gridpoints

A time series analysis of the baseline pairs was conducted to determine if the temporal behavior of the pairs would yield useful information. This information could be used as a measuring stick for system performance if it shows low frequency trends or fluctuations. However, no pattern could be deduced from the time series which would prove useful in this goal. Figures (21) through (23) illustrate that there is no fluctuation among the absolute difference matched pairs which would indicate when the system was operating efficiently or otherwise. In these plots, the upper plot is the standard baseline pairing and the lower plot is the best correlated pairing from the correlation analysis in the last section. As one would expect, the best correlated pairings yield a more compact dispersion of matched points.

Additionally, a check of the matched pair differences for the gridpoint pairings was performed to determine if any biases were present in the radial data. Since all biases found were less than 4 cm/s, no significant systematic errors were present. Table 2 lists the results.

Gridpoint Pairings (angles reference to east)	Corr. Value	RMS Diff (cm/s)	Bias (cm/s)
SCruz(286/18)-Pt.Piños(110/18)	0.5358	22.0185	-3.9305
SCruz(286/18)-Pt.Piños(120/18)	0.7465	17.2012	-1.0787
SCruz(326/18)-M.Land.(150/11)	0.5599	15.0348	2.1322
SCruz(326/18)-M.Land.(155/11)	0.5995	14.6513	3.0551
Pt.Piños(055/12)-M.Land.(230/11)	0.3599	19.9438	-0.4679
Pt.Piños(060/12)-M.Land.(245/11)	0.6692	14.8123	-0.8333

Table 2. Summary of correlation, RMS difference, and bias analysis for baseline gridpoint pairs and best correlated gridpoint pairs.

2. Comparison with Moored Current Observations

A unique opportunity existed to conduct further checks with the standard baseline gridpoint for the Santa Cruz-Point Piños baseline due to the close proximity of the M1 mooring. This position is shown in Figure (6). An Acoustic Doppler Current Profiler (ADCP) time series of currents in the vicinity of the M1 mooring at a depth of 8 m were compared with the best correlated pairings from the Santa Cruz and Point Piños sites. Figure (24) is a scatter plot of matched pairs (data included for the times when velocities from both the ADCP and CODAR system were available). The upper two panels compare all available data (upper left panel"u"-component and the upper right panel "v"-component). The lower two panels compare data from the mooring against sub-sampled

data, which are those pairs occurring at times when the best correlated Santa Cruz-Point Piños baseline comparison (Figure 21) had an absolute value less than 10 cm/s.

It is important to note that even though there is an approximate difference in measuring depths of 7 m and real differences are expected, the level of baseline agreement does not appear to be related to overall system performance as measured against the moored current observations. By systematically eliminating CODAR data with a high absolute value difference, no appreciable change was seen in the slope of the best fit line through the scatter, in the correlation between CODAR-derived and moored current components, or in the spread about the best-fit line. Therefore, the accuracy due to the combined sources of noise of CODAR/SeaSonde appears to be on the order of 15 cm/s vice the published 4 cm/s spectral resolution.

D. RADIAL ERROR ESTIMATE ANALYSIS

In addition to estimates of radial current magnitudes from the sea echo, the CODAR algorithms provide estimates of the error (or uncertainty) of the radial currents based on assumptions about the statistical nature of the backscatter data (Lipa and Barrick, 1983). Analysis of the radial error estimates provided in the radial data files was conducted to determine the usefulness of the estimates in determining the reliability of the data used to create radial current maps as well as total current vector maps. The radial error estimates, if useful, should indicate when one or more of the network sites is operating at below system specifications.

The assumption in utilizing these data is that if a given radial velocity has an associated high radial error estimate, that radial velocity could be filtered out and the system's

accuracy improved. This assumption also implies that the radial velocity "flagged" with a high radial error estimate by the system would, on average, have a high absolute value difference when compared to the corresponding radial velocity value from the opposite site along the baseline. If this is not the case, it would suggest that the assumptions made about the statistical nature of the backscatter spectra are incorrect. Two means were used to determine the usefulness of the radial error estimates, histogram plots and absolute value difference versus radial error estimate scatter plots.

1. Histogram Plots

Histogram plots were used to illustrate the distribution of radial error estimates for each of the three radar sites. Figure (25) shows representative examples of histograms illustrating the radial errors and their distributions. All three sites showed an expected distribution of observations with respect to errors: most errors are less than 12 cm/s from all three sites with relatively few occurrences of large errors. However, an unidentified problem exists in the Moss Landing system. Data from that site includes a large number of off-scale (9999 cm/s) error vales. In order to keep scales consistent among the three sites, all error estimates greater than 150 cm/s were binned together at 150 cm/s in the histograms in Figure (25). Apart from the off-scale error values in the Moss Landing data, the error estimates are of the same order as the radial current estimates. The remaining question is whether or not large error estimates correlate with large errors as inferred from the baseline comparisons.

2. Scatter Plots

Scatter plots were used to illustrate the spread of the absolute value differences of matched pairs versus radial error estimate values. The expected distribution, if the

radial error estimates are useful, would have the matched pairs with the highest radial error estimates having the highest absolute value differences. In Figures (26) through (28) all radial error estimate values greater than 150 cm/s were filtered out in order to maintain conformity among the axis values. The upper plots are representative of the baseline gridpoint pairings and the lower plots are the best correlated gridpoint pairings. For these comparisons, the larger of the two error estimates at a given time is plotted along the abscissa. Unfortunately, as is illustrated in Figures (26) through (28), the matched pairs having relatively high associated errors have a wide range of absolute value differences from a few cm/s to as high as approximately 100 cm/s. No correlation exists between absolute value difference and error estimates, therefore, we cannot use one to predict the other.

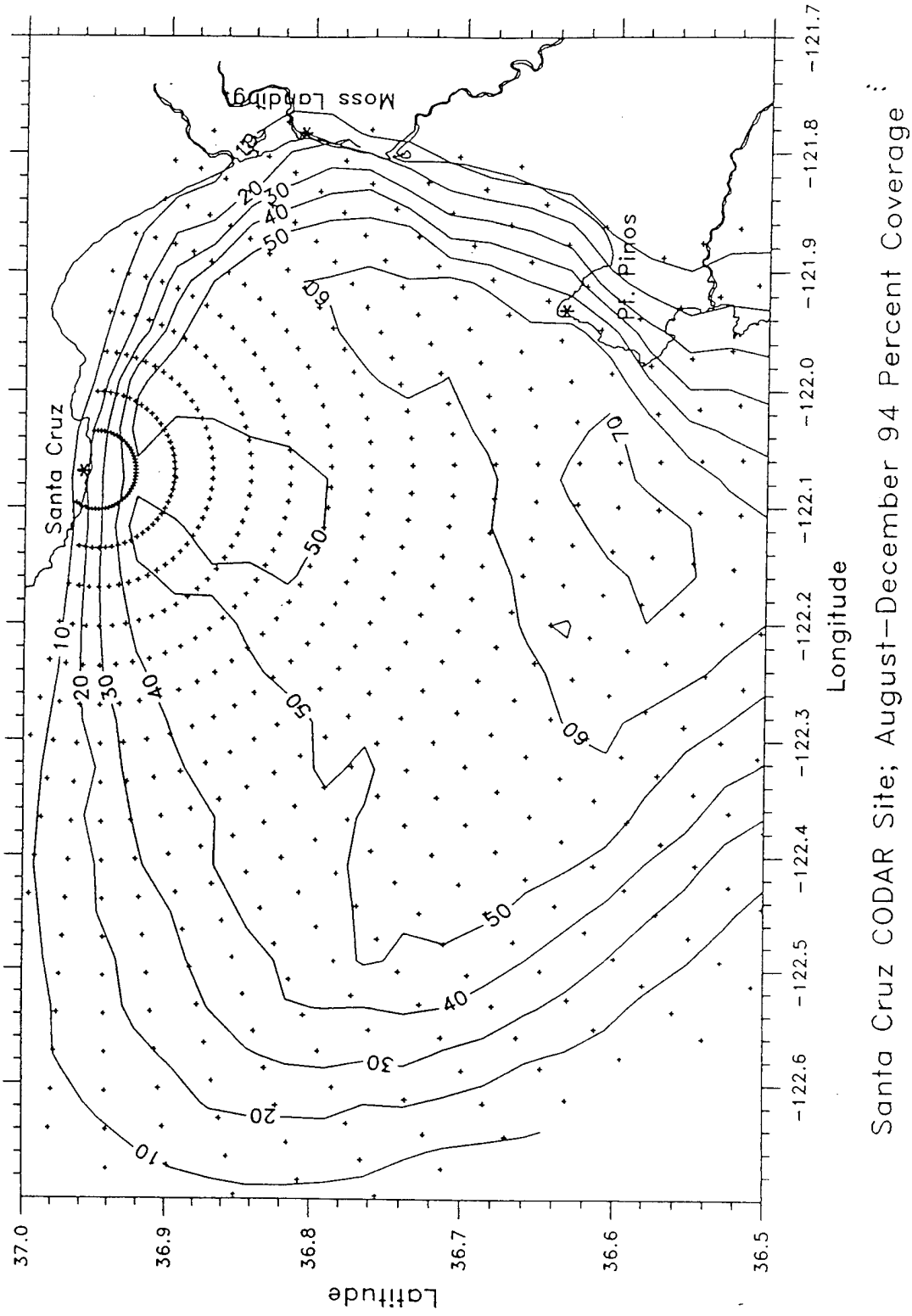

Figure 8. Percent coverage map for the period of August through December 1994 from the Santa Cruz SeaSonde site.

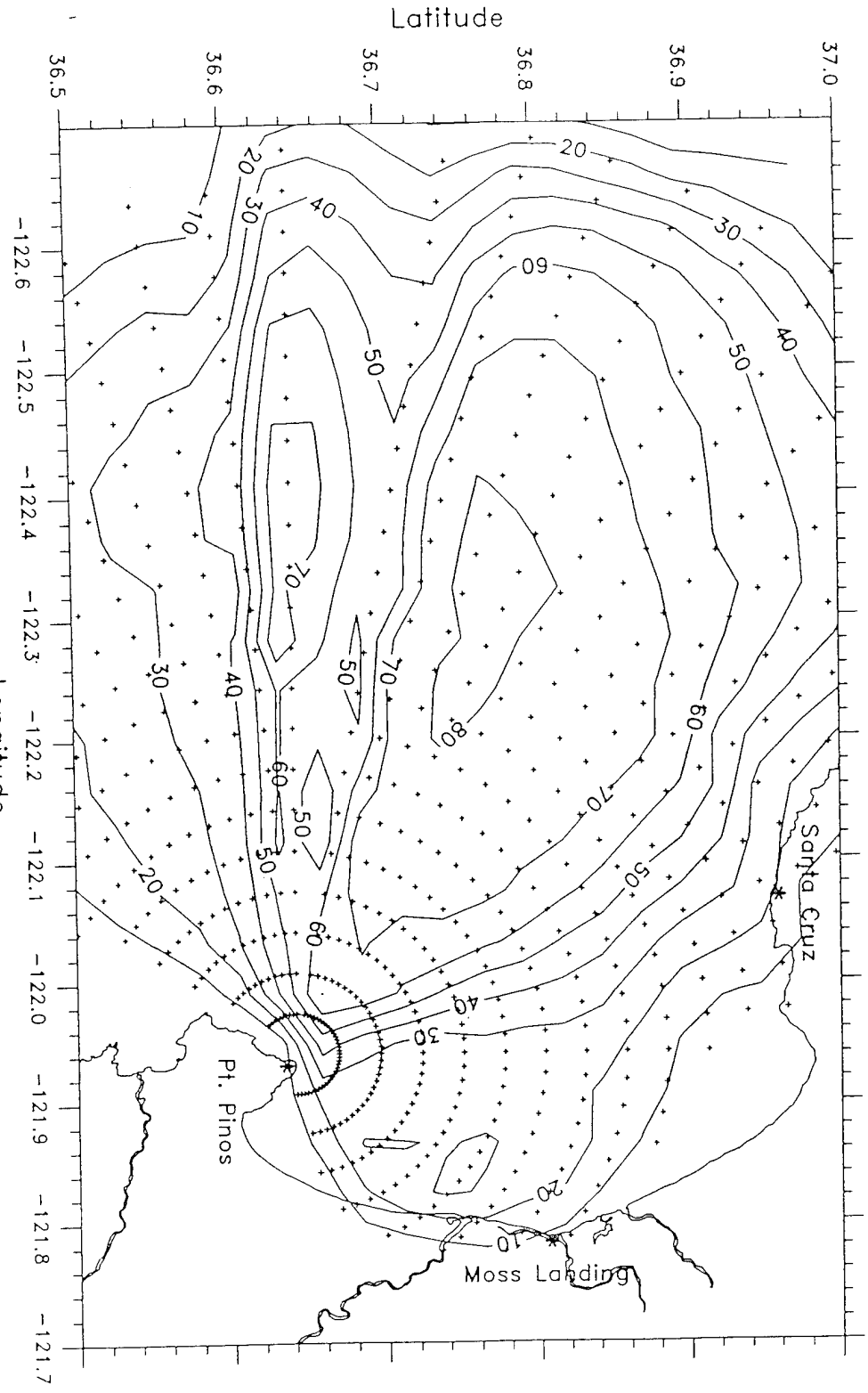

Point Pinos CODAR Site; August-December 94 Percent Coverage.

Figure 9. Percent coverage map for the period of August through December 1994 for the Point Piños SeaSonde site.

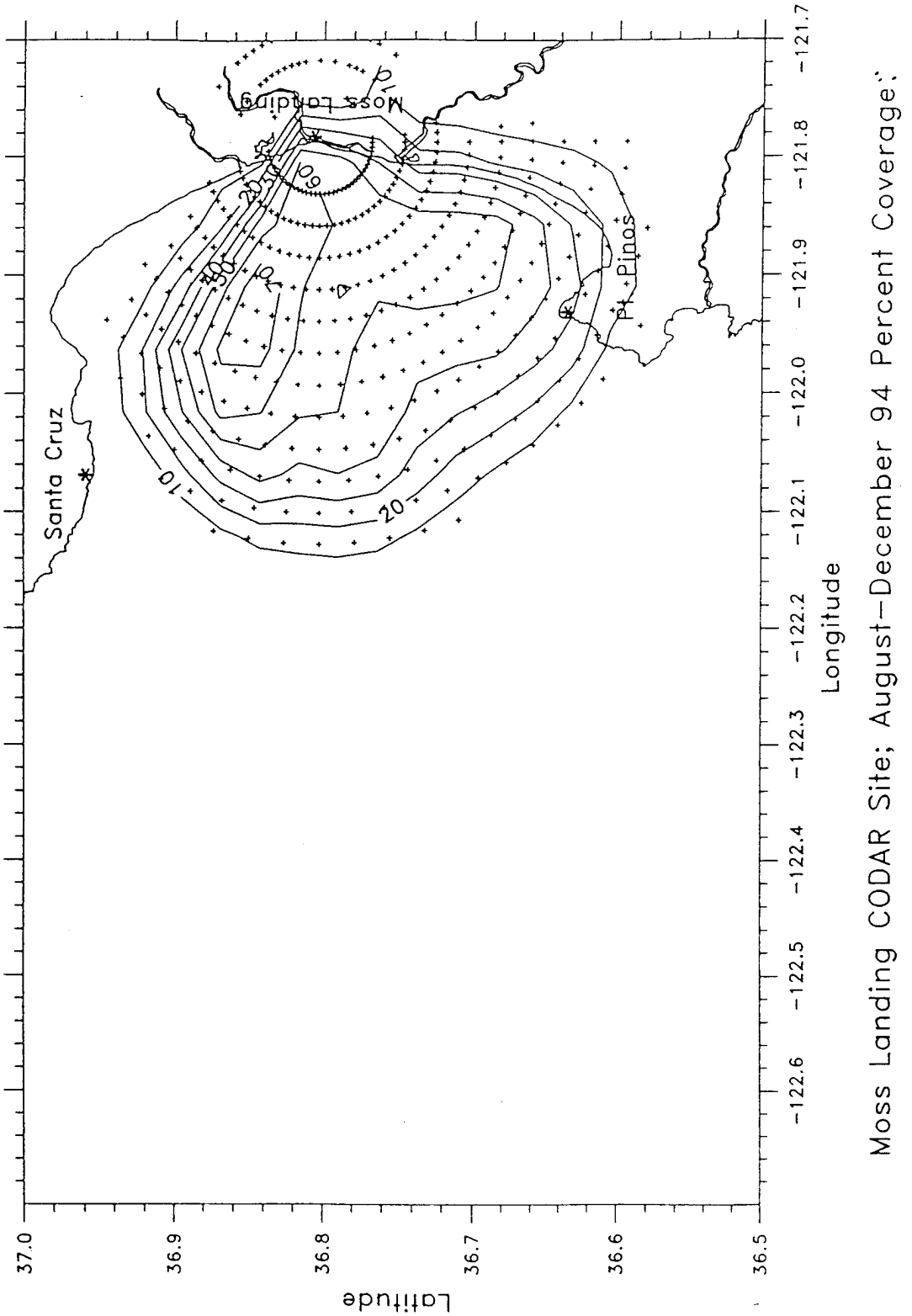

Figure 10. Percent coverage map for the period of August through December 1994 for the Moss Landing CODAR site.

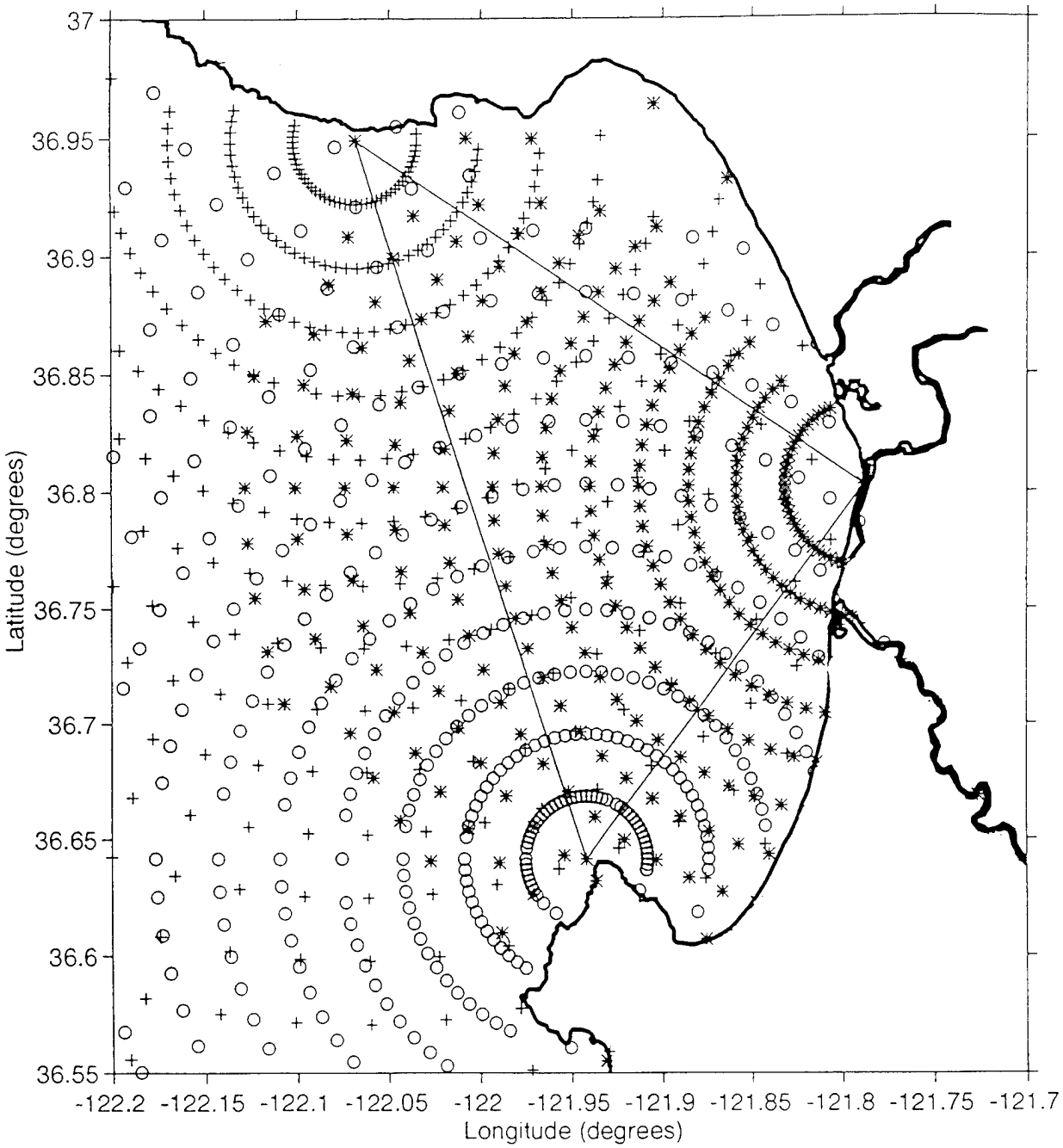

Figure 11. Radial bin distribution from the Santa Cruz (+), Point Piños (o), and Moss Landing (*) HF radar sites around Monterey Bay. Solid lines denote nominal baseline between station pairs.

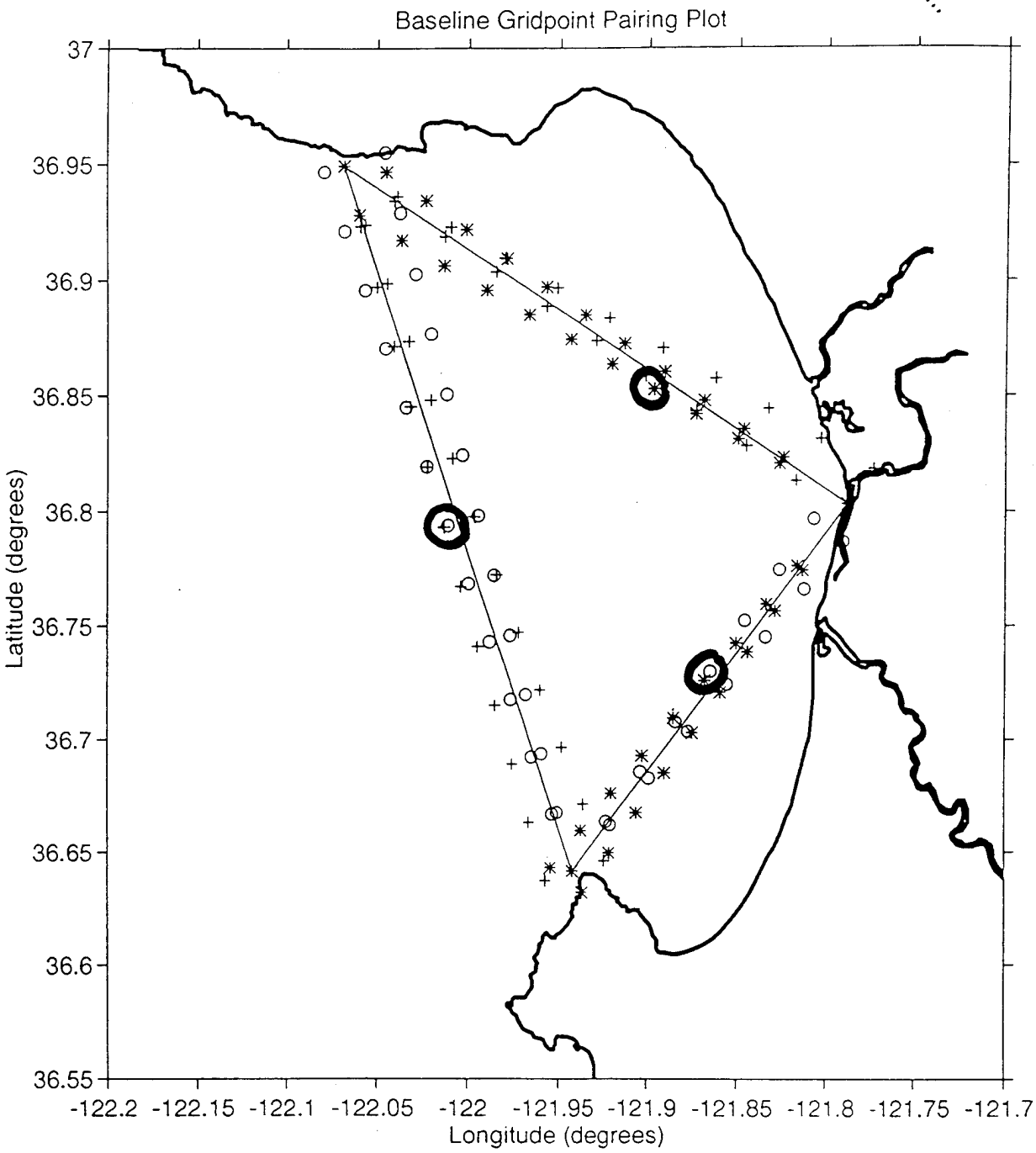

Figure 12. Baseline gridpoint locations. The three pairs analyzed in this study are circled.

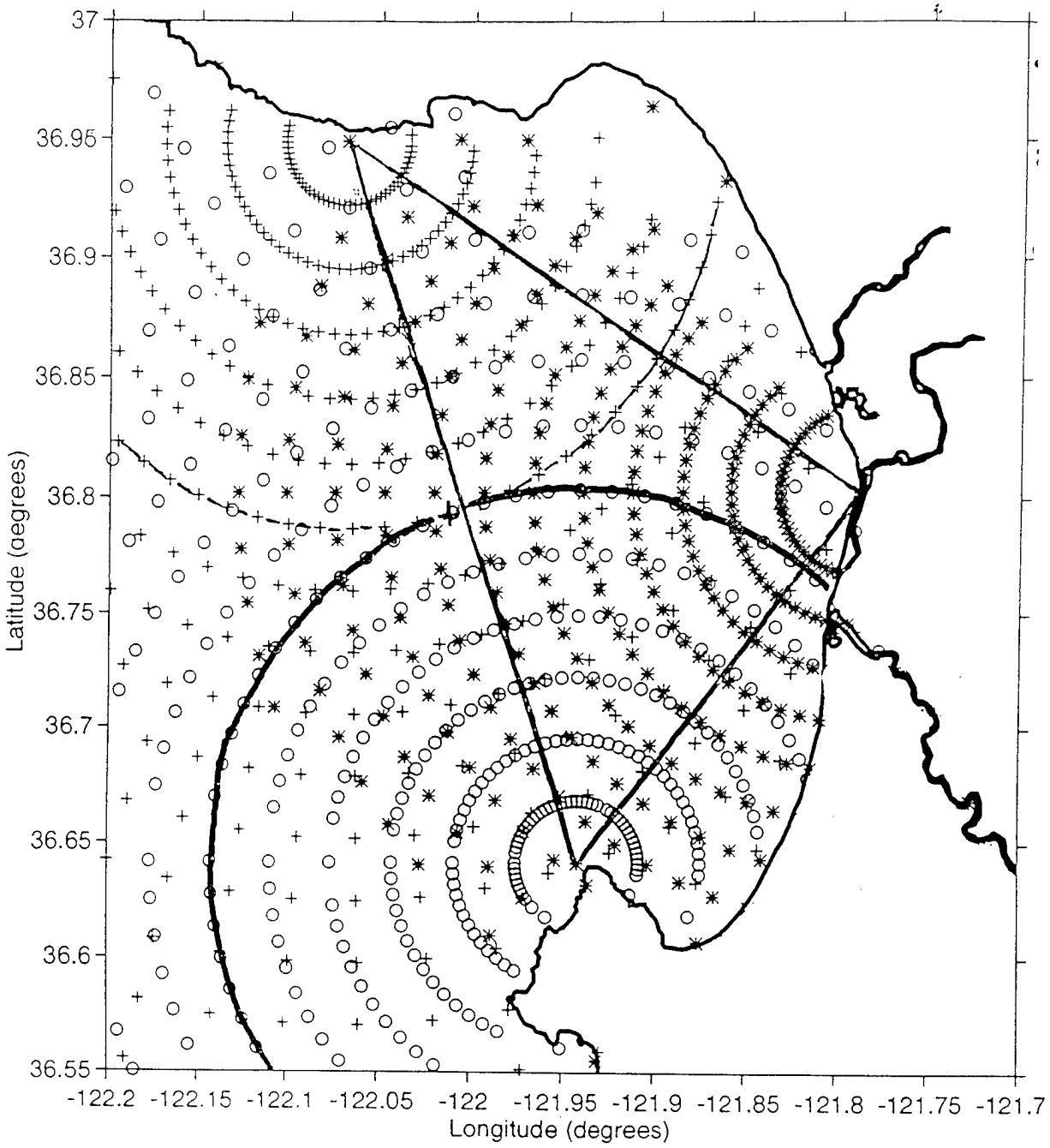

Figure 13. Illustration of process used to conduct correlation and RMS difference analysis among all three baselines. In this example, all Santa Cruz radial bins are compared to all Point Piños radial bins along their respective 18 km range arcs depicted in the figure.

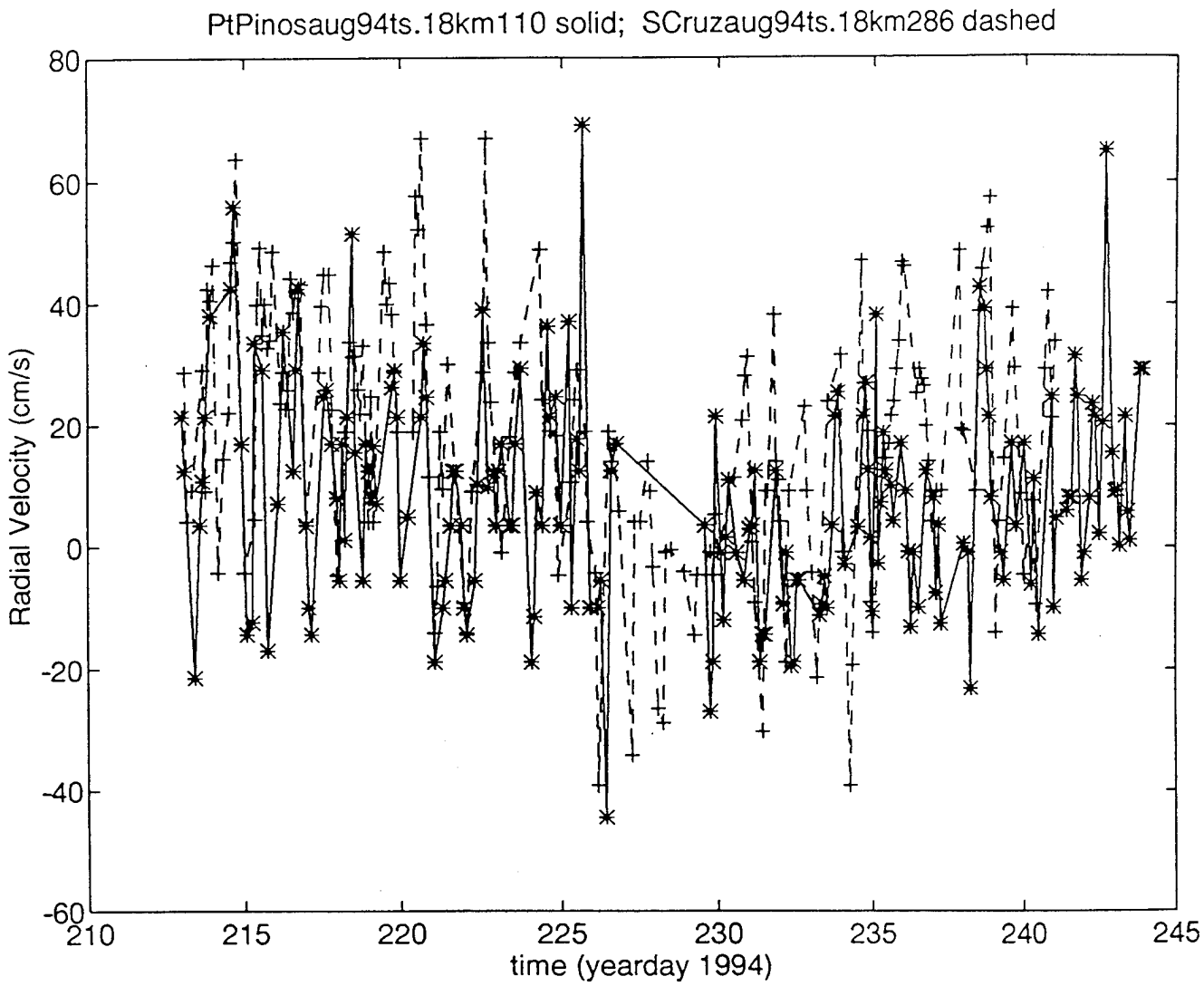

Figure 14. Raw data time series for the standard gridpoint pairing along the Santa Cruz-Point Piños baseline for the month of August 1994.

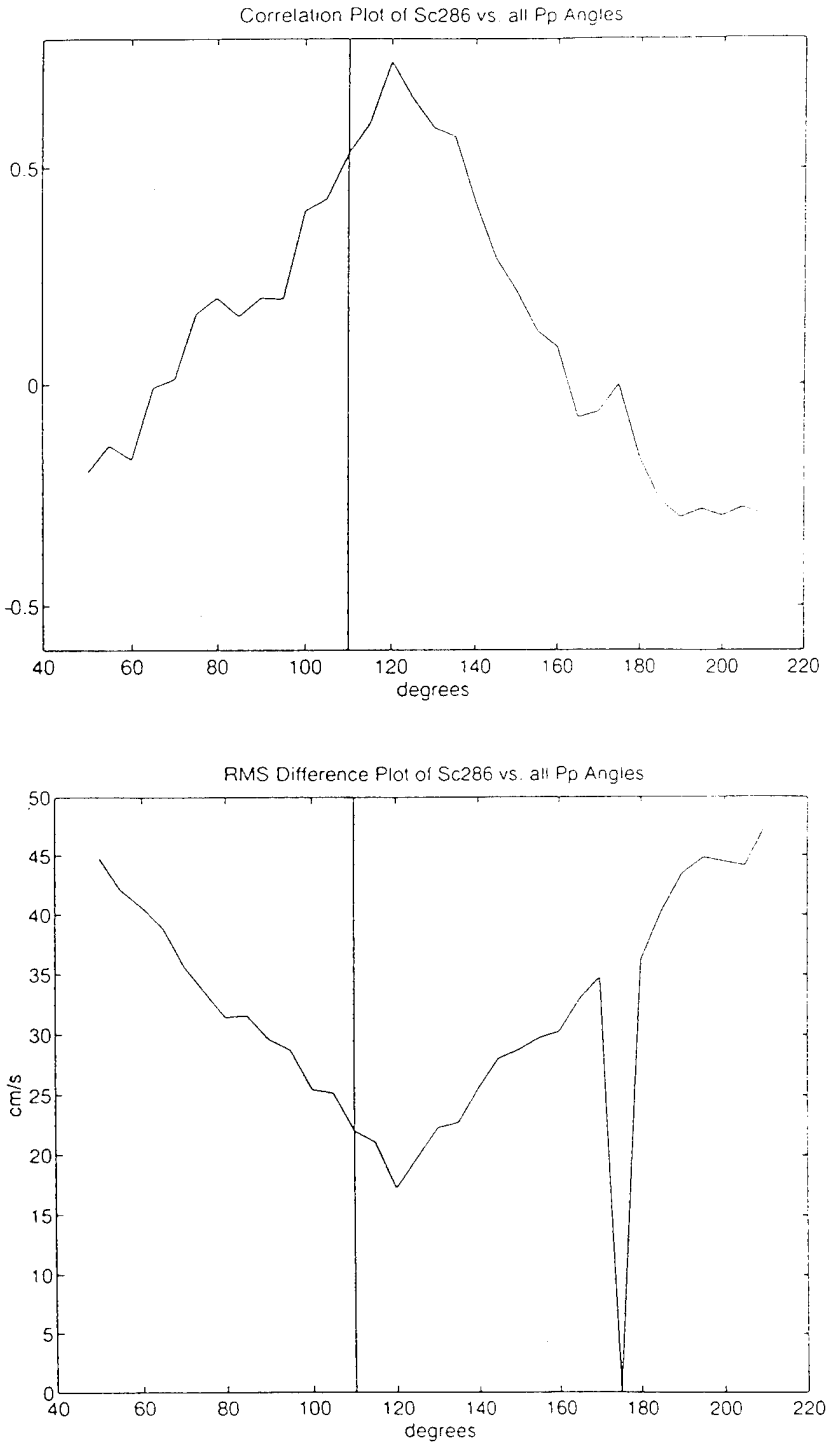

Figure 15. Correlation (upper panel) and RMS difference (lower panel) plots of the Santa Cruz SeaSonde site as compared to all radial 18 km bins from the Point Piños SeaSonde site. Results are plotted as a function of angle from the Point Piños site for the standard gridpoint from Santa Cruz. Angle denoted by the vertical bar is the expected angle from the standard baseline pairs.

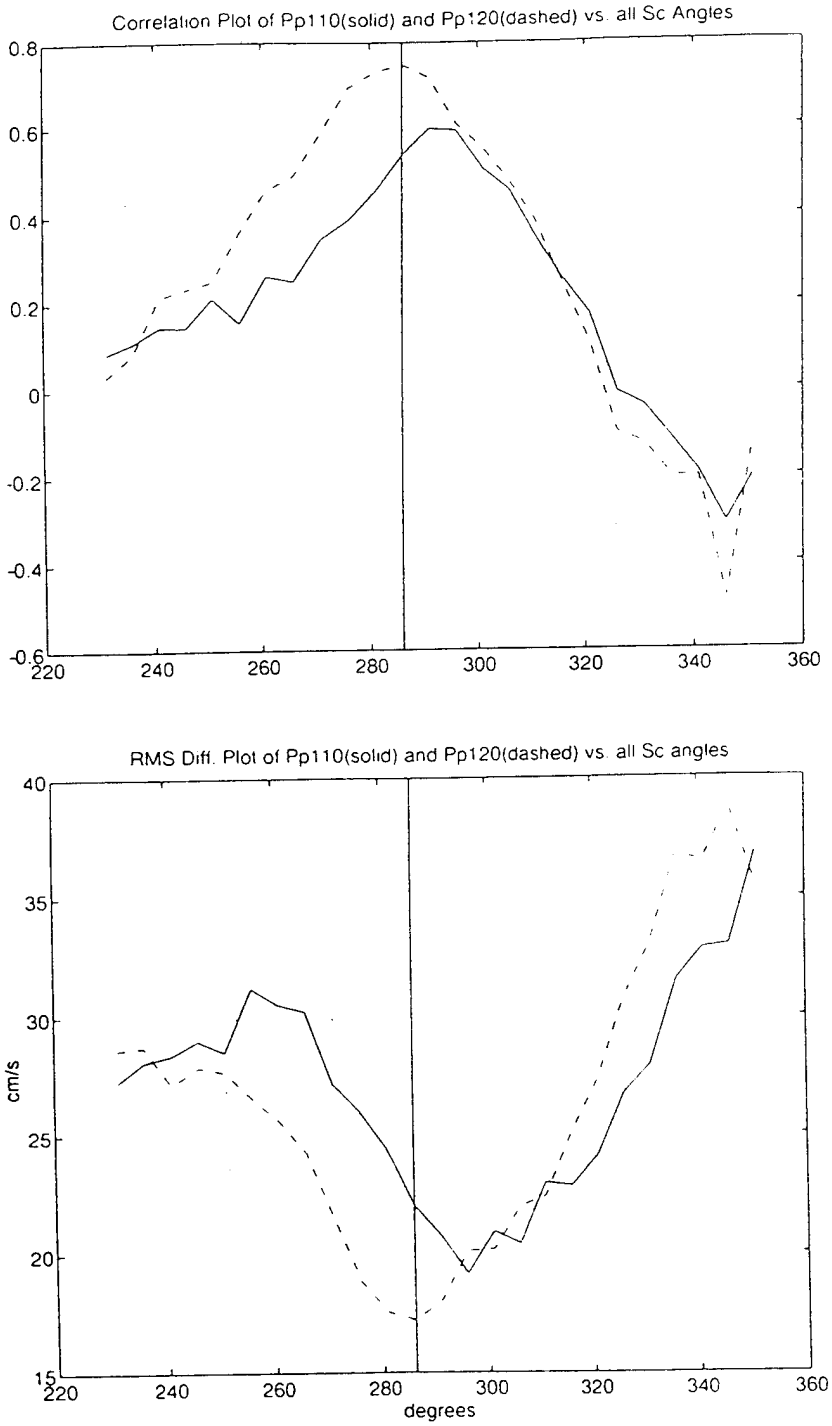

Figure 16. Correlation (upper panel) and RMS difference (lower panel) plots of the Point Piños SeaSonde site as compared to all radial 18 km bins from the Santa Cruz SeaSonde site. Results are plotted as a function of angle from the Santa Cruz site for the standard (solid) and the best correlated (dashed) gridpoint from Point Piños. Angle denoted by the vertical bar is the expected angle from the standard baseline pairs.

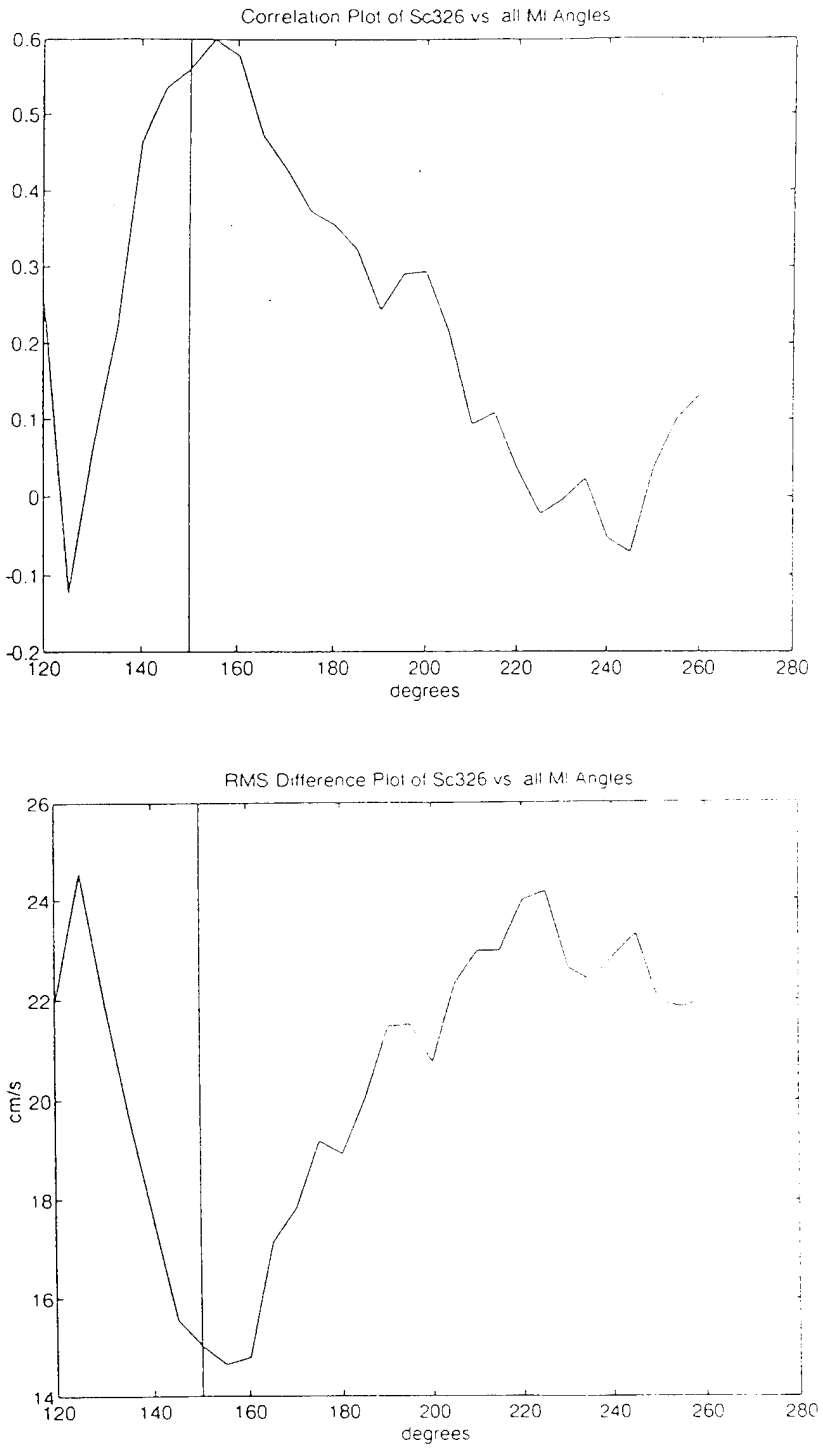

Figure 17. Correlation (upper panel) and RMS difference (lower panel) plots of the Santa Cruz SeaSonde site as compared to all 11.1 km radial bins from the Moss Landing CODAR site. Results are plotted as a function of angle from the Moss Landing site for the standard gridpoint from Santa Cruz. Angle denoted by the vertical bar is the expected angle from the standard baseline pairs.

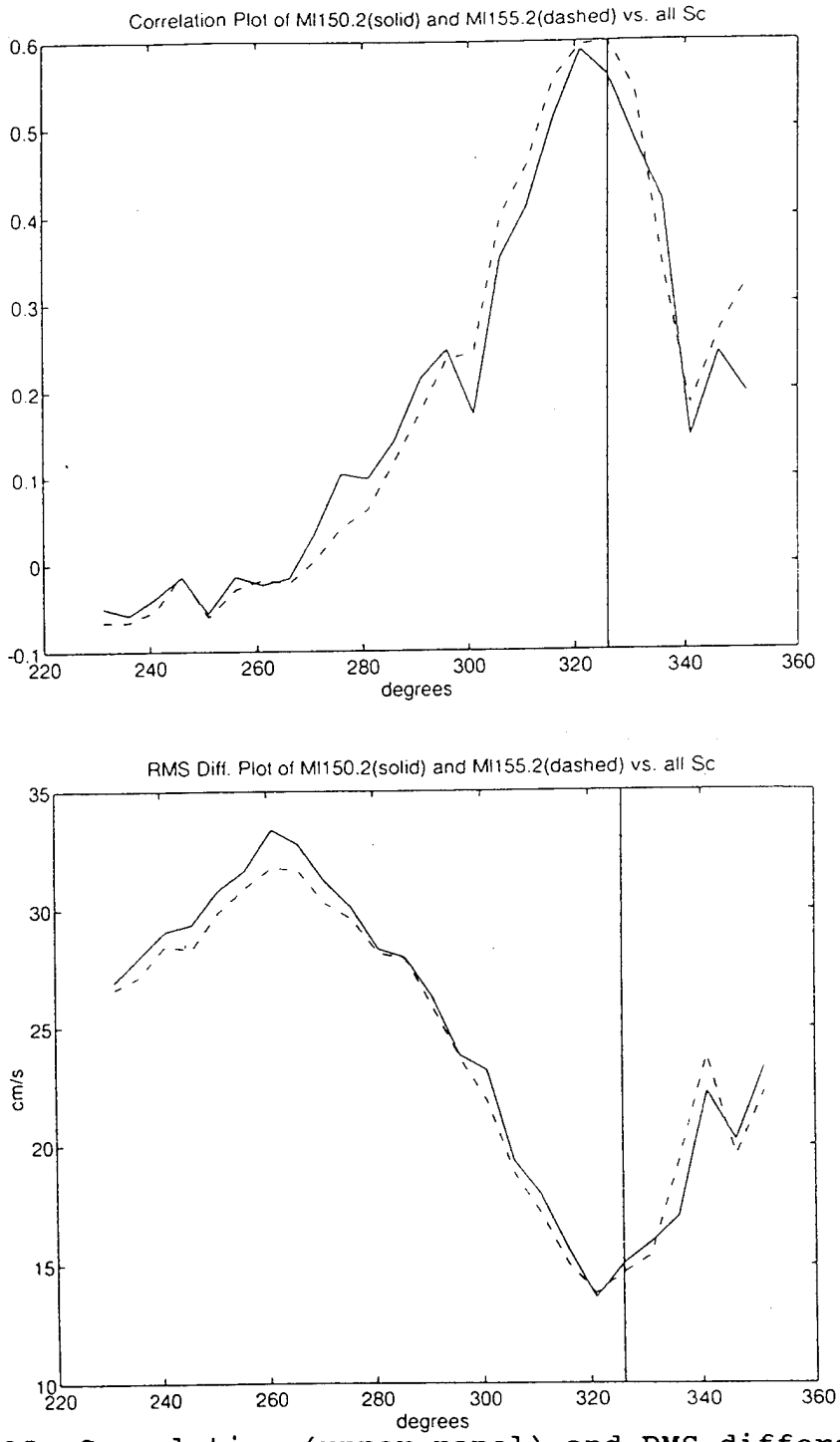

Figure 18. Correlation (upper panel) and RMS difference (lower panel) of the Moss Landing CODAR site as compared to all radial 18 km bins from the Santa Cruz SeaSonde site. Results are plotted as a function of angle from the Santa Cruz site for the standard (solid) and best correlated (dashed) gridpoint from Moss Landing. Angle denoted by the vertical bar is the expected angle from the standard baseline pairs.

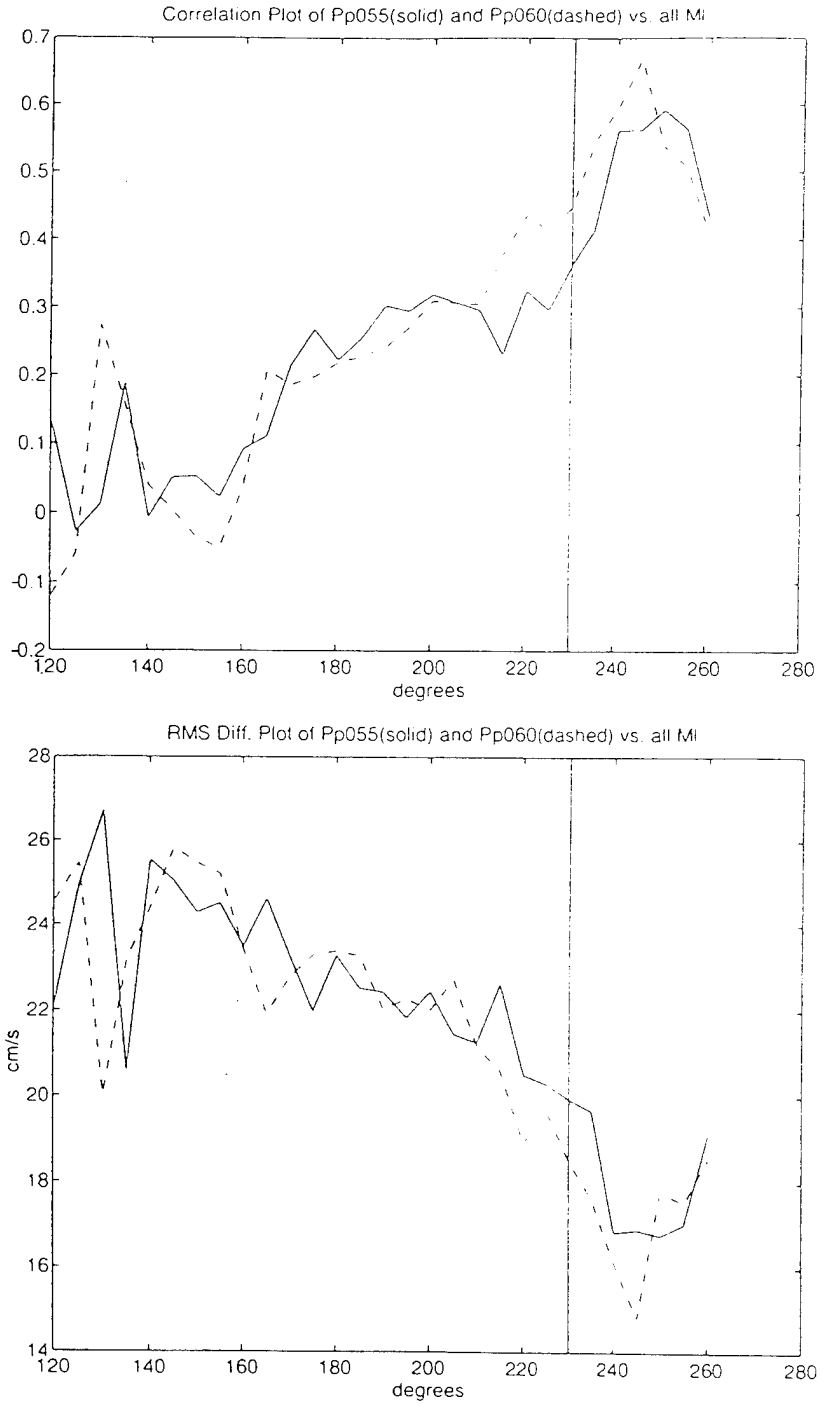

Figure 19. Correlation (upper panel) and RMS difference (lower panel) plots of the Point Piños SeaSonde site as compared to all radial 11.1 km bins from the Moss Landing CODAR site. Results are plotted as a function of angle from the Moss Landing site for the standard (solid) and best correlated (dashed) gridpoint from Point Piños . Angle denoted by the vertical bar is the expected angle from the standard baseline pairs.

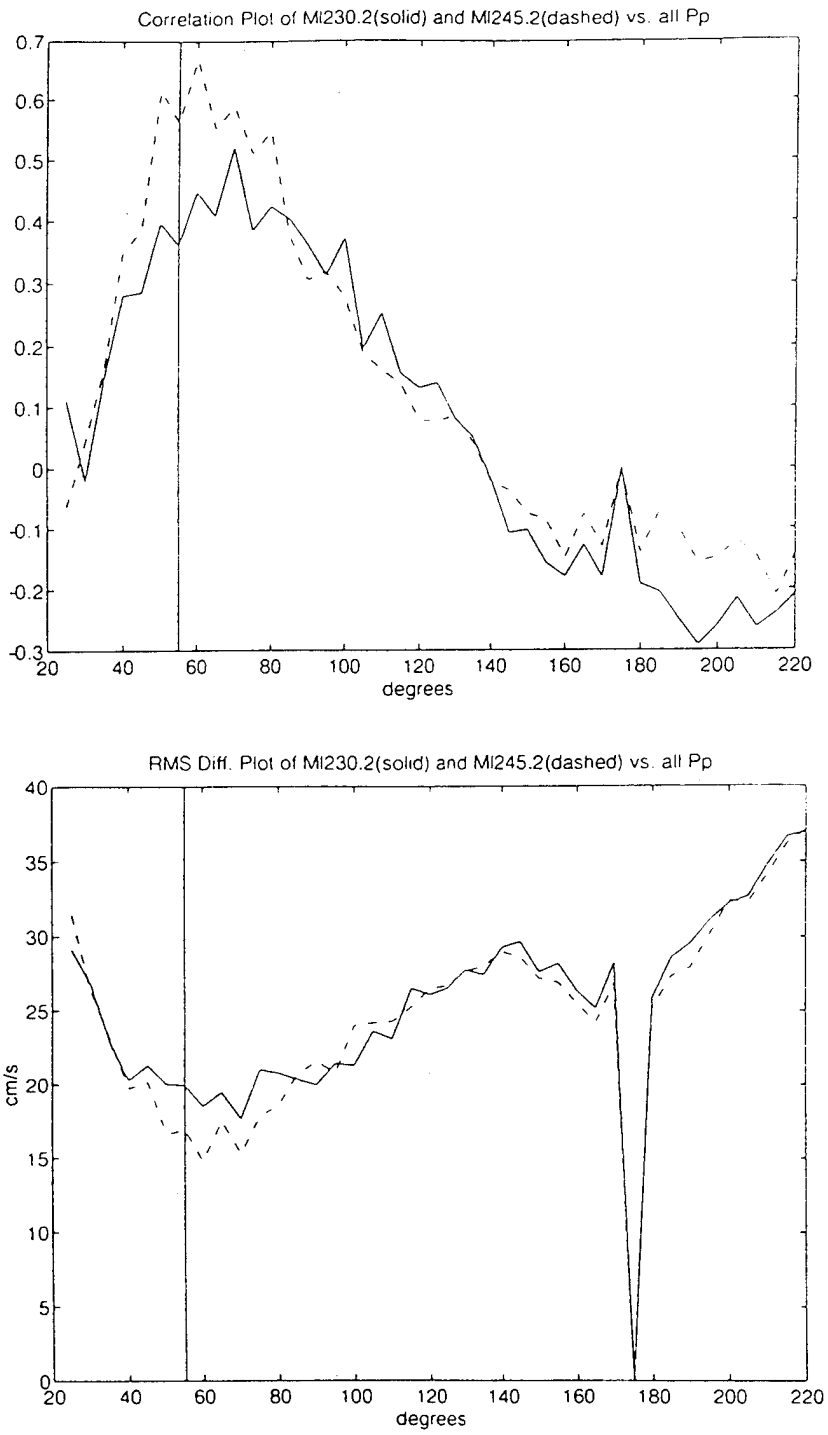

Figure 20. Correlation (upper panel) and RMS difference (lower panel) plots of the Moss Landing CODAR site as compared to all radial 12 km bins from the Point Piños SeaSonde site. Results are plotted as a function of angle from the Point Piños site for the standard (solid) and best correlated (dashed) gridpoint from Moss Landing. Angle denoted by the vertical bar is the expected angle from the standard baseline pairs.

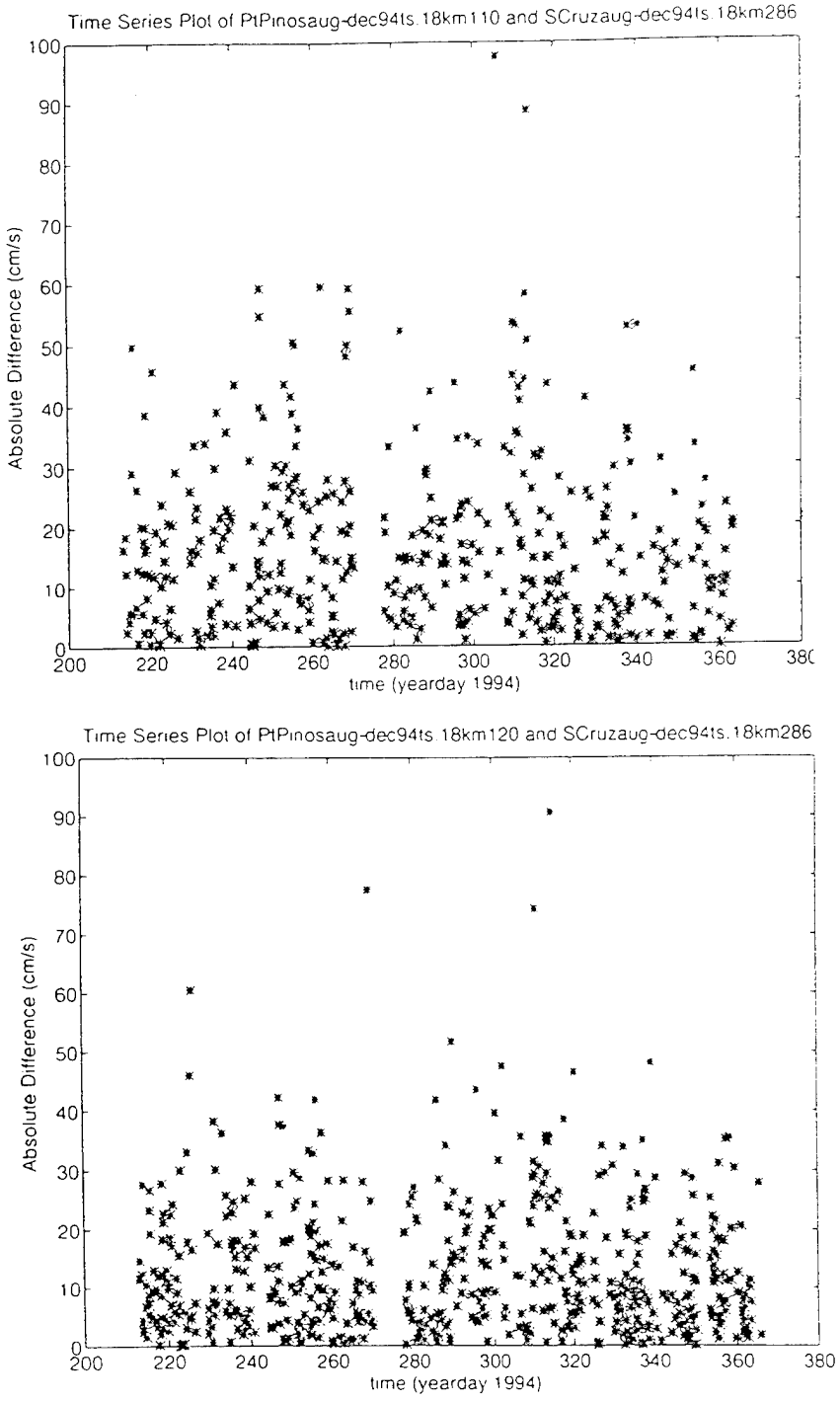

Figure 21. Time series plots of the Santa Cruz-Point Piños standard baseline pairings (upper panel) and the best correlated gridpoint pairings (lower panel).

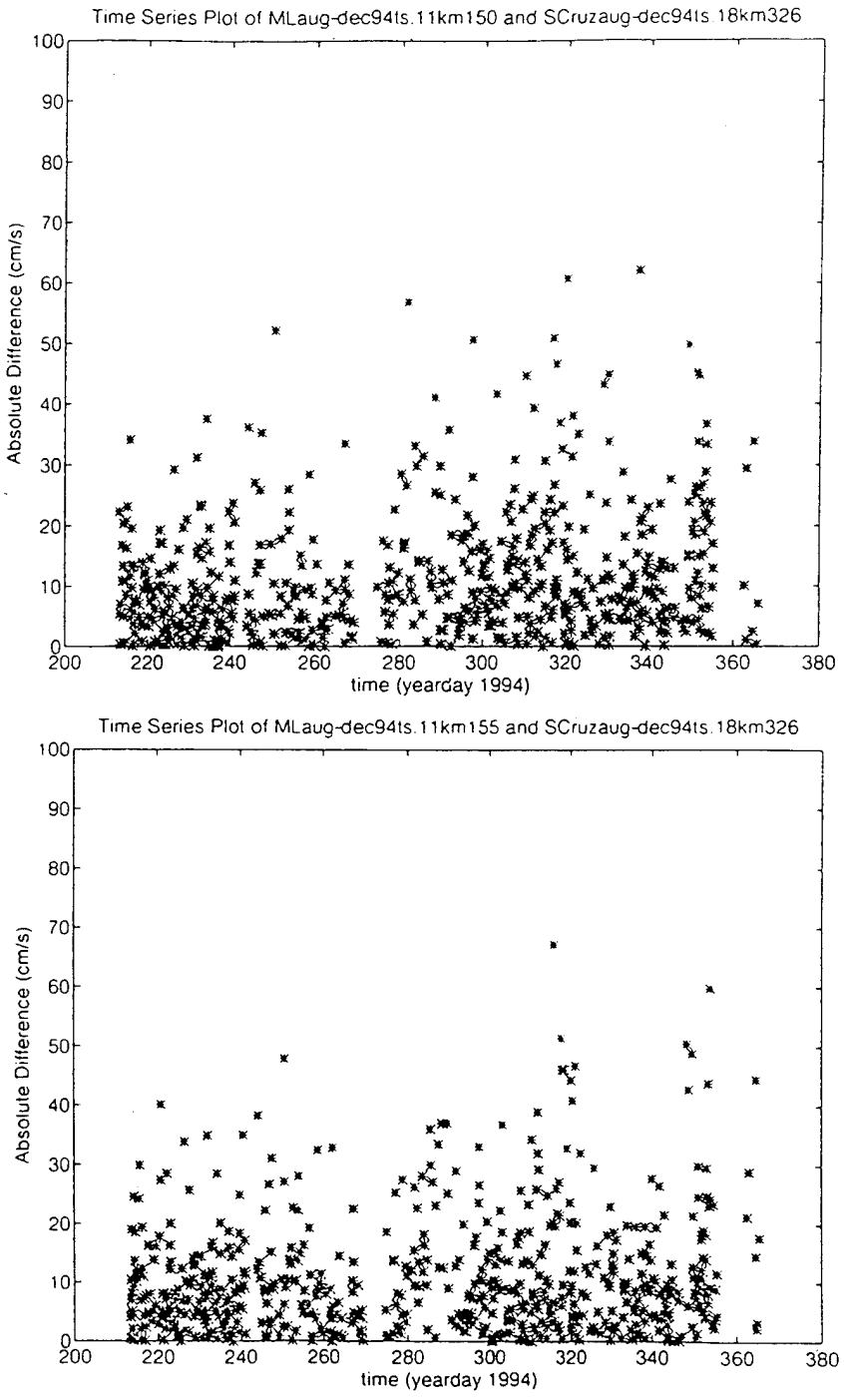

Figure 22. Time series plots of the Santa Cruz-Moss Landing standard baseline gridpoint pairings (upper panel) and the best correlated gridpoint pairings (lower panel).

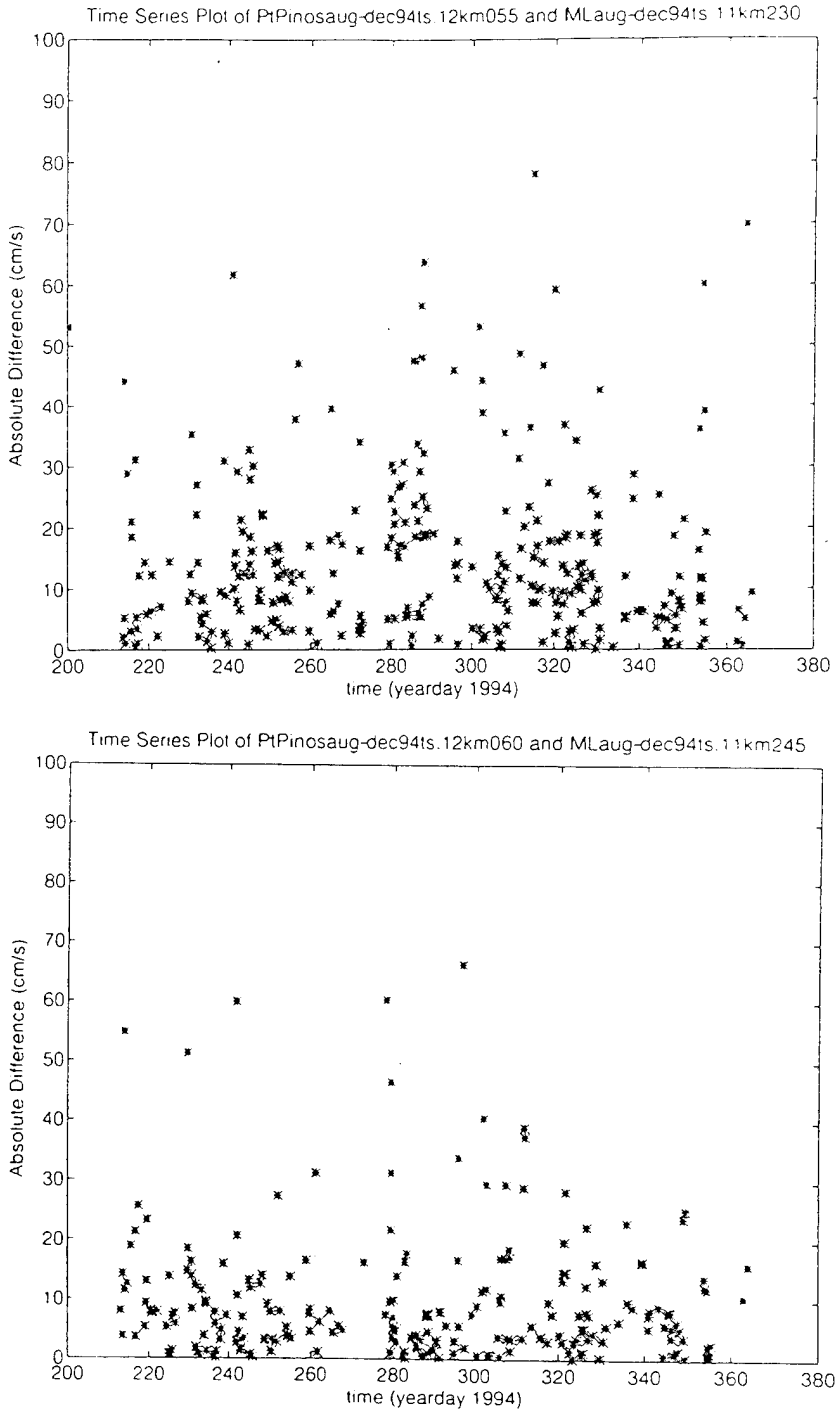

Figure 23. Time series plots of the Point Piños-Moss Landing standard baseline gridpoint pairings (upper panel) and the best correlated gridpoint pairings (lower panel).

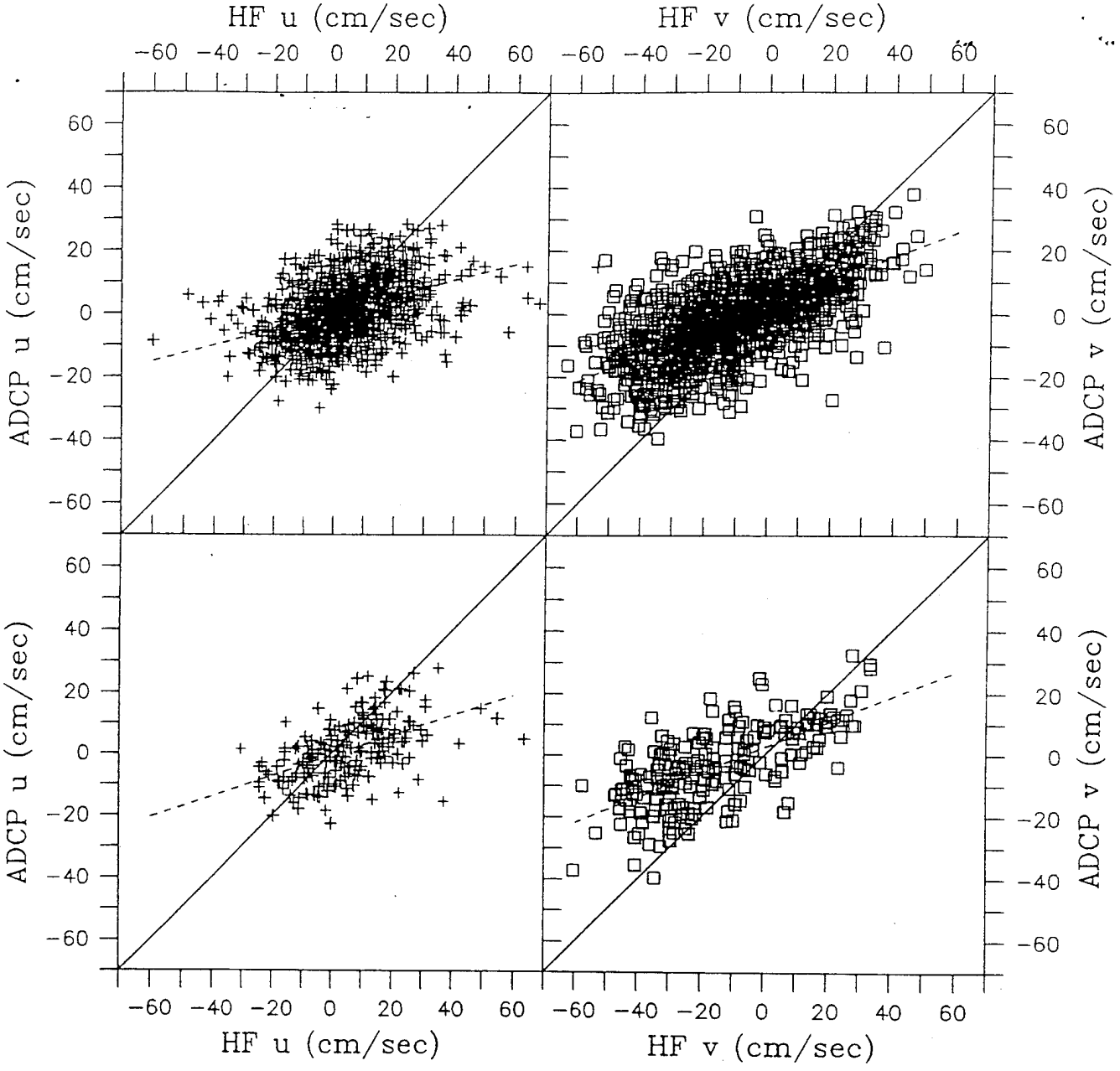

Figure 24. Scatter plot comparisons of M1 mooring ADCP current measurements vs. CODAR system current measurements. The upper pair of panels represent the "u" and "v" component comparisons for the full data comparisons for matched data. The lower pair of panels represent the "u" and "v" component comparisons for the filtered CODAR data (all data with differences greater than 10 cm/s removed) and corresponding data from the ADCP current mooring.

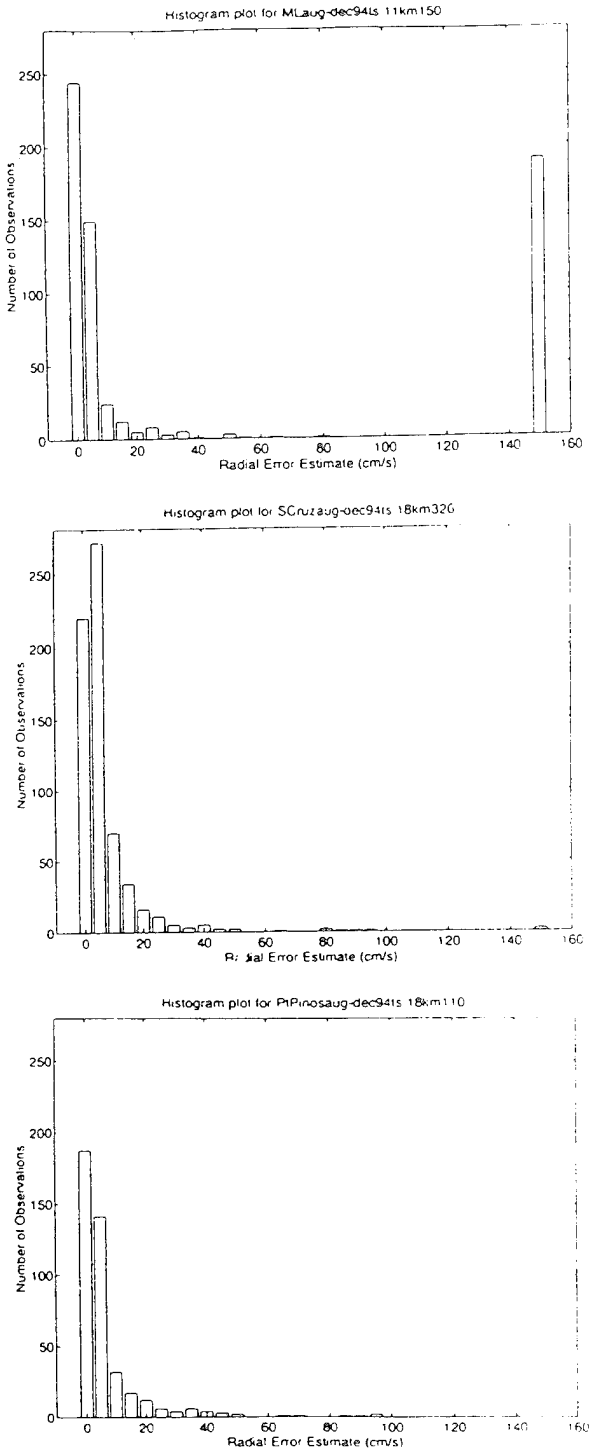

Figure 25. Representative examples of histogram plots from each of the three network sites depicting number of observations vs. radial error estimates. All values greater than 150 cm/s are binned together at 150 cm/s.

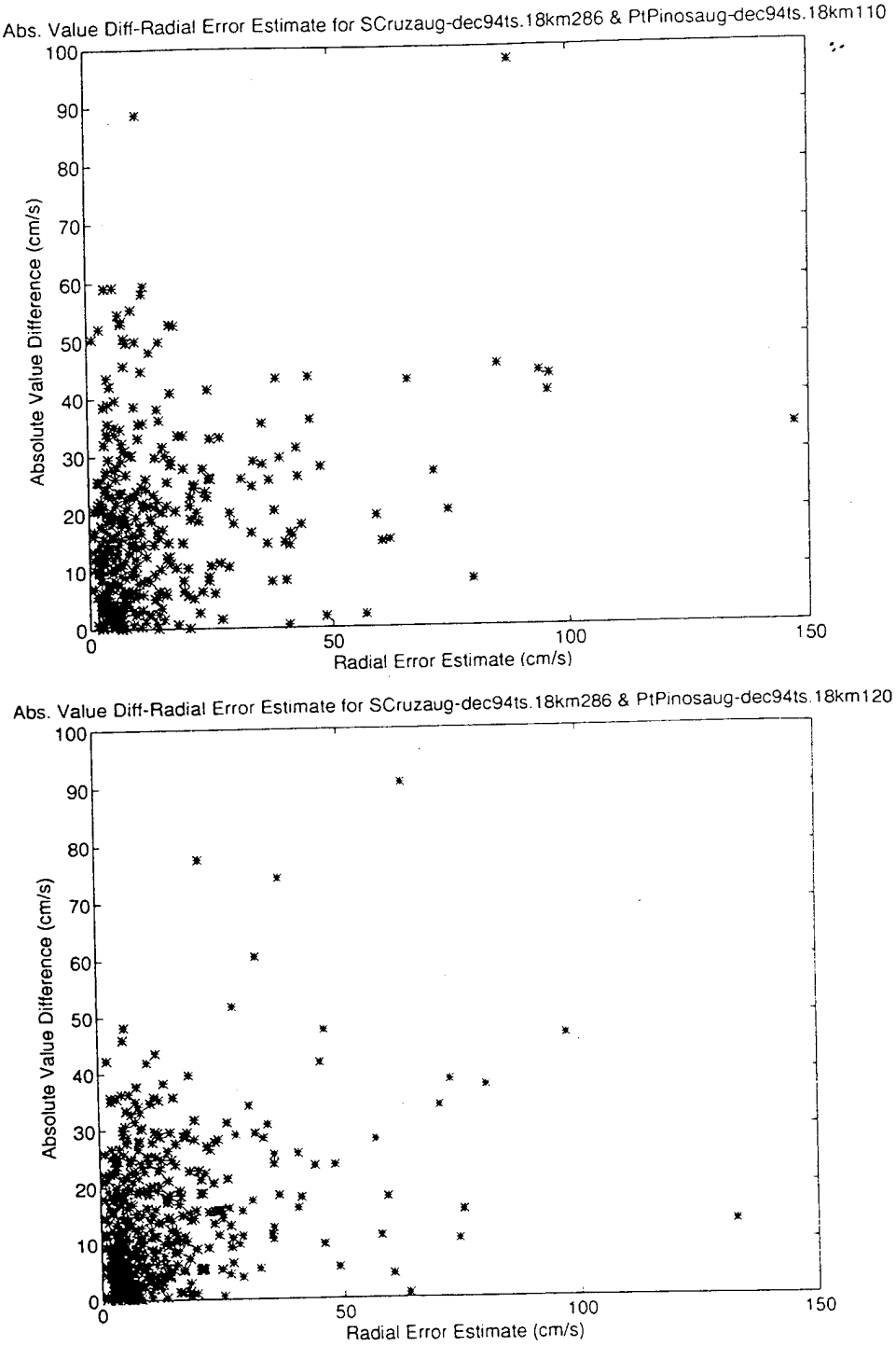

Figure 26. Absolute value difference vs. radial error estimate scatter plots for the Santa Cruz-Point Piños 18 km standard gridpoint pairing (upper panel) and the best correlated 18 km gridpoint pairing (lower panel).

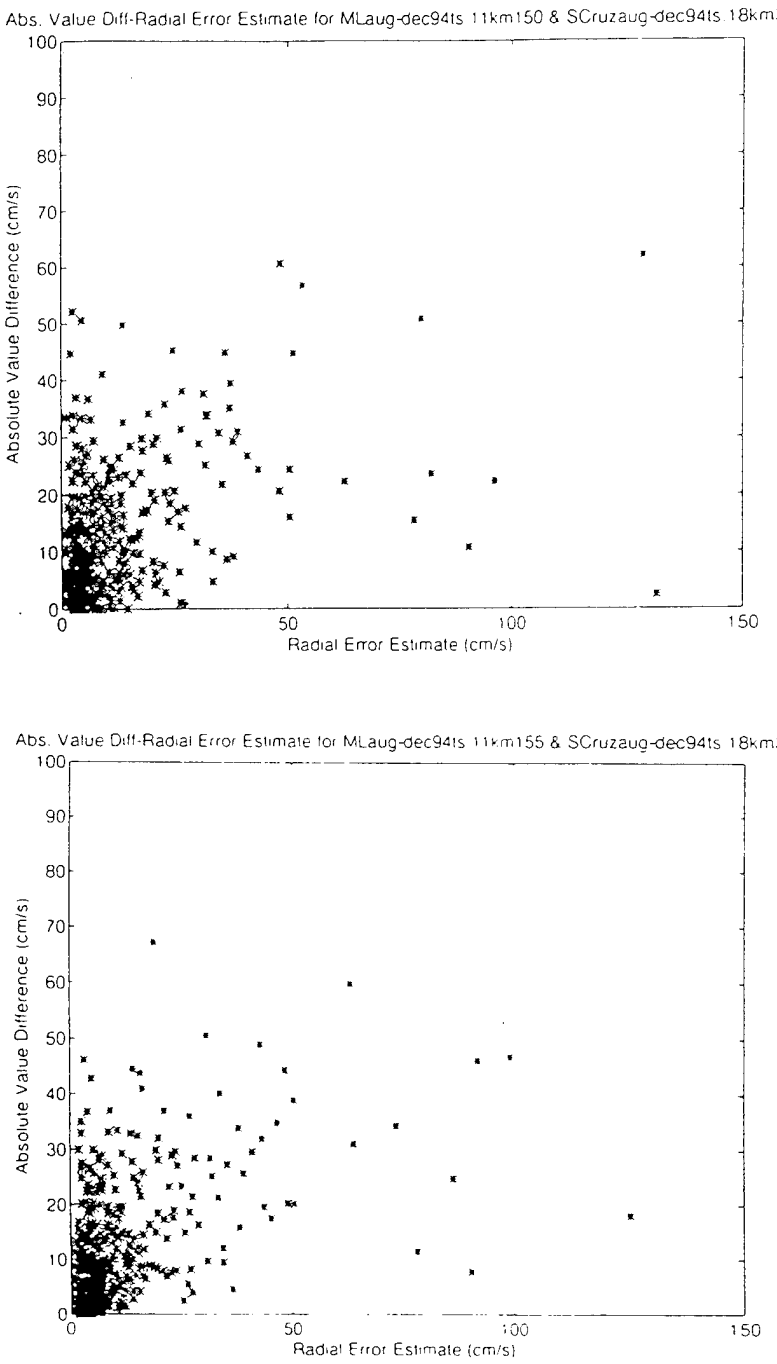

Figure 27. Absolute value difference vs. radial error estimate scatter plots for the Santa Cruz (18 km)-Moss Landing (11.1 km) standard baseline gridpoint pairing (upper panel) and the best correlated gridpoint pairing (lower panel).

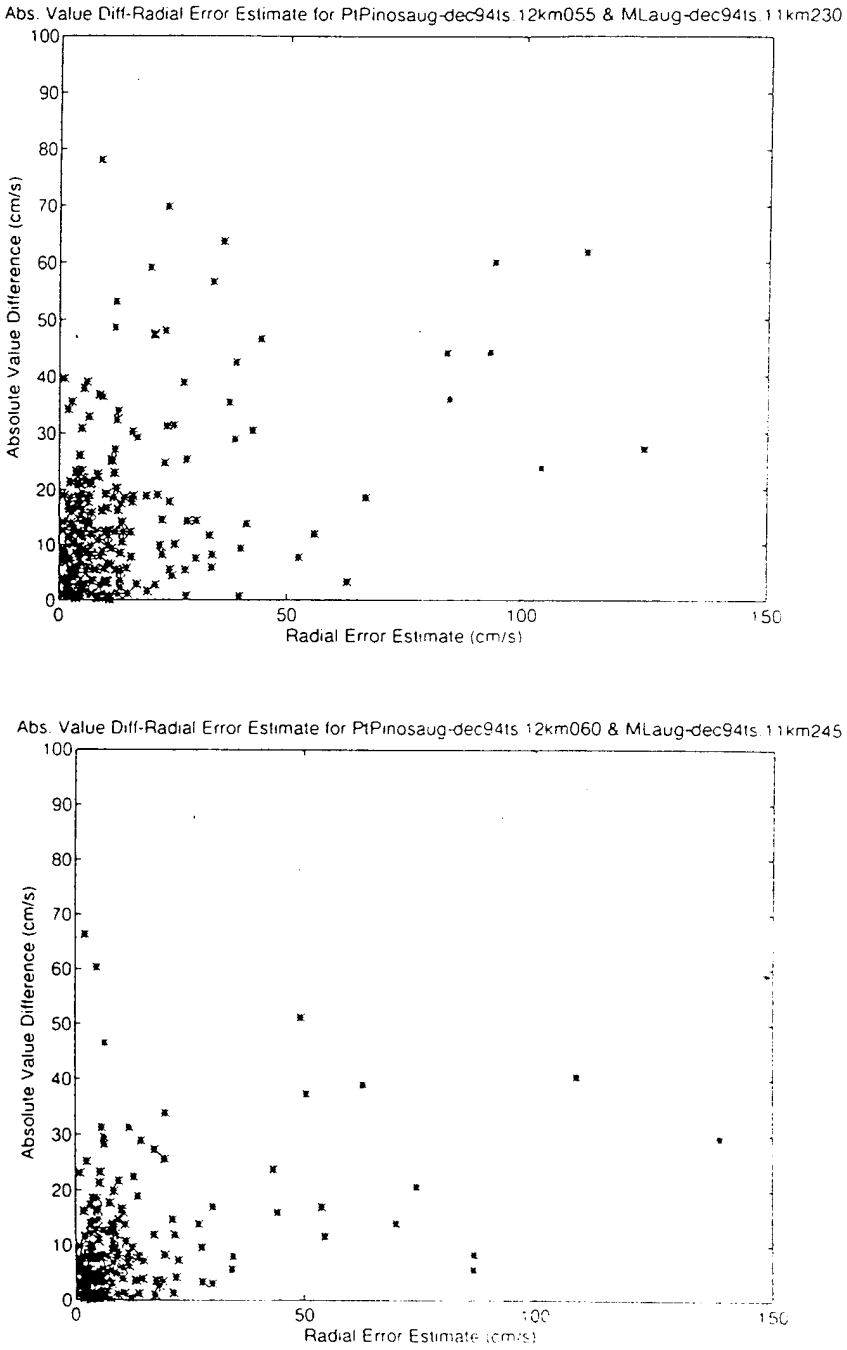

Figure 28. Absolute value difference vs. radial error estimate scatter plots for the Point Piños (12 km)-Moss Landing (11.1 km) standard baseline gridpoint pairing (upper panel) and the best correlated gridpoint pairing (lower panel).

III. SUMMARY

Statistical analyses of the radial current velocity data from each of the three CODAR network sites around Monterey Bay were conducted for the five month period from 01 August 1994 through 31 December 1994. This amounted to nearly 5400 radial current files. The aim of this study, which took a step backwards with respect to previous studies using total current vector maps, was to establish the reliability of the CODAR network by analyzing the radial current velocity data which comprises the basis of the total current vector maps. Examination of the long term antenna coverage patterns suggested that distorted antenna patterns associated with each of the antenna systems exist. This study examined the RMS differences and correlations between baseline gridpoint pairings and the best correlated gridpoint pairings. This reveal that, at the three baseline positions chosen, the best correlated pairings were not those along the baselines as they should have been. Additionally, the RMS differences found, even among the best correlated gridpoint pairings, revealed higher than expected values. The last main focus of the study analyzed the usefulness of the radial error estimates provided in the data as a measuring stick for system performance. It was determined that the radial error estimates were not correlated with system performance as inferred from baseline comparisons.

A. CORRELATION AND RMS DIFFERENCE ANALYSIS

Results from the correlation and RMS difference analysis revealed previously unknown information concerning the CODAR network deployed around Monterey Bay. In two of the three systems, significant pointing errors were found to exist. The

Point Piños errors were found to be on the order of ten degrees in the counterclockwise direction, whereas, the Moss Landing site errors were on the order of five degrees in the counterclockwise direction. Unlike the other two sites, the Santa Cruz site exhibited no pointing errors in the baseline checks. As a local means of correction from the user's perspective, rotation of the Point Piños radial data field ten degrees clockwise and the Moss Landing radial data field five degrees clockwise *before* computing total vector maps would alleviate the misalignment along two of the three baselines. Figure (29) is a summary illustration of the pointing errors discovered and the subsequent radial data field shifts required to correct the misalignments locally.

In order to ensure that the results from this process were consistent all along the baselines as opposed to just three distinct positions examined, additional RMS difference and correlation analyses were conducted on additional baseline positions. An example of these findings is shown in Figures (30) and (31), which depict data from an additional gridpoint pairing along the Santa Cruz-Point Piños baseline. The results are consistent with those found at the other standard gridpoint pairing along that baseline. (The same pointing errors and RMS difference magnitudes were present as those found for the Santa Cruz 286°/18 km and Point Piños 110°/18 km pairing.)

Recently, CODAR Ocean Sensors, LTD., made three sets of bearing measurements to transponders placed at Santa Cruz and Moss Landing. This afforded an electronic check of pointing errors found in this study. Checks could be made from the Santa Cruz and Point Piños SeaSonde sites but not the Moss Landing CODAR site due to limitations of the older system. Therefore, only information concerning pointing errors could be made for Santa Cruz and Point Piños. It is also important to note that these measurements were made after the Point

Piños antenna was rotated June 6, 1995, and that pointing errors detected are not directly related to ones discovered in the August to December 1994 data. Results reported by these direct transponder measurements are as follows: 4.5° counterclockwise error from Point Piños toward Santa Cruz, 5.75° counterclockwise error from Point Piños toward Moss Landing, and 9.9° counterclockwise error from Santa Cruz toward Moss Landing. These results are reasonable except for the pointing error determined for Santa Cruz, which directly contradicts the findings of this study. Further transponder measurements should be made after similar correlations and RMS difference measurements can be made for data collected after 6 June 1995.

Pointing errors aside, another disturbing fact was revealed in the RMS differences between baseline pairs. Even among the best correlated pairings, the RMS differences were found to be on the order of 14 cm/s or greater, substantially higher than expected. In conducting a bias analysis for theses pairings, no systemic errors were discovered due to biasing of radial current data from the three sites. Table 2 summarizes the correlations, RMS differences, and biases found for the baseline gridpoint pairs and for the best correlated pairs.

B. TIME SERIES OF BASELINE PAIRS

By investigating long time series comparisons between the baseline gridpoint pairs and the best correlated gridpoint pairs, the temporal behavior of the matched pairs was examined to determine if a pattern was discernable which would indicate when individual systems were operating efficiently or less than specifications. Unfortunately, this analysis did not yield any pattern which could be used to measure network

performance. As expected, the best correlated pairs had a tighter grouping of matched pairs with respect to absolute value differences over time. The mean of the data is consistent with the earlier determined RMS differences found in the data from the respective network sites.

Moored ADCP current measurements from the M1 mooring were compared with the nearby radar-derived total vector currents described by Paduan and Rosenfeld (1995) using additional information from the Santa Cruz-Point Piños standard baseline gridpoint. Even after eliminating CODAR measurements with a high absolute value difference, no appreciable change was seen in the slope of the best fit line through the scatter, in the correlation between CODAR-derived and moored current components, or in the spread about the best fit line. Therefore, the level of baseline agreement does not appear to be related to overall network performance as measured by moored current observations.

C. RADIAL ERROR ESTIMATE ANALYSIS

In evaluating the radial error estimates provided in the data from the respective systems, the expectation was that the estimates would be useful in determining when erroneous data was present in the data. This would provide a useful means of screening bad data out of the radial current data files. However, this analysis revealed that the error estimates are not useful. As is seen in the scatter plots (Figures (26) through (28)), the radial current velocities having a high associated radial error estimate did not necessarily have a correspondingly high absolute value difference. In fact, radial current velocities having a high error estimate varied in absolute value difference from a few cm/s to approximately 100 cm/s. Thus establishing a radial error estimate threshold

above which all radial velocities would be filtered out would not improve the output product of the network systems appreciably as judged by baseline comparisons. Although the distribution of error estimates was reasonable in most cases, frequent off-scale values in the data from the Moss Landing CODAR also points to a breakdown of the statistical assumptions made to produce the error estimates (Lipa and Barrick, 1983).

D. RECOMMENDATIONS

Based on the types of analyses conducted in this study and the results obtained, the following recommendations are made to improve future performance of CODAR-type HF radar systems around Monterey Bay and elsewhere:

- Antenna calibration measurements should be conducted in situ for every HF radar deployment using direct transponder measurements where possible and the CODAR-type direction finding algorithms should be augmented to accept realistic corrections based on the measured antenna patterns.

- Long term radial current coverage patterns should be monitored because they reflect the repeated results of the CODAR direction finding algorithms under the influence of the actual antenna beam patterns and the backscatter characteristics of the local ocean area.

- Directional wave measurements should be conducted within the radar field of view and correlated with coverage patterns to assess the, possible, role of wave direction in the preferred directions output by the

CODAR direction finding algorithms. (As a first order proxy for wave direction, it may be possible to use wind direction measurements within the radar field of view to begin this process.)

- In the absence of direct antenna pattern measurements, correlation analyses between radial gridpoints along and off the network baselines should be used to test for biases in the CODAR direction finding algorithms. The results of this study suggest that improvements to the accuracy of the radar-derived total vector current maps in Monterey Bay during the period from August through December 1994 could be obtained by rotating the radial current data from Point Piños 10° clockwise and the radial current data from Moss Landing 5° clockwise *before* computing the total current vector maps.

- The specific reference angles used in the direction finding algorithms for the CODAR site at Moss Landing during the August through December 1994 should be determined and it should be verified that the baseline reference angle used points toward the Point Piños SeaSonde site as was assumed by the total vector current processing algorithms. The rotation correction implied by the correlation analyses conducted in this study show the baseline angle to have actually pointed toward the decommissioned CODAR site at Hopkins Marine Laboratory, which was used to determine the reference angle in 1992. Hence, the correction inferred for the Moss Landing system could either be the result of actual distortions of the antenna beam patterns or, possibly, a mistake in the reference angle.

- Simulation studies should be conducted using the CODAR

direction finding algorithms applied to synthetic spectra produced from realistic, known ocean wave and current fields to look for biases in the pointing results that can explain the patterns observed in the long term coverage maps. Such simulation studies should also be conducted to assess the level of random errors in the measurement that may explain the high RMS differences (~15 cm/s) observed for radial current pairs along the baseline between the two radar systems.

- The assumptions involved in the derivation of radial error estimates should be reviewed and revised because the error estimates provided by the present CODAR algorithms are not correlated with system performance as inferred from baseline comparisons.

- The older-generation CODAR system at Moss Landing should be replaced with a SeaSonde system in order to improve the network coverage within Monterey Bay and to provide for the ability to conduct direct transponder antenna calibration tests at all three sites.

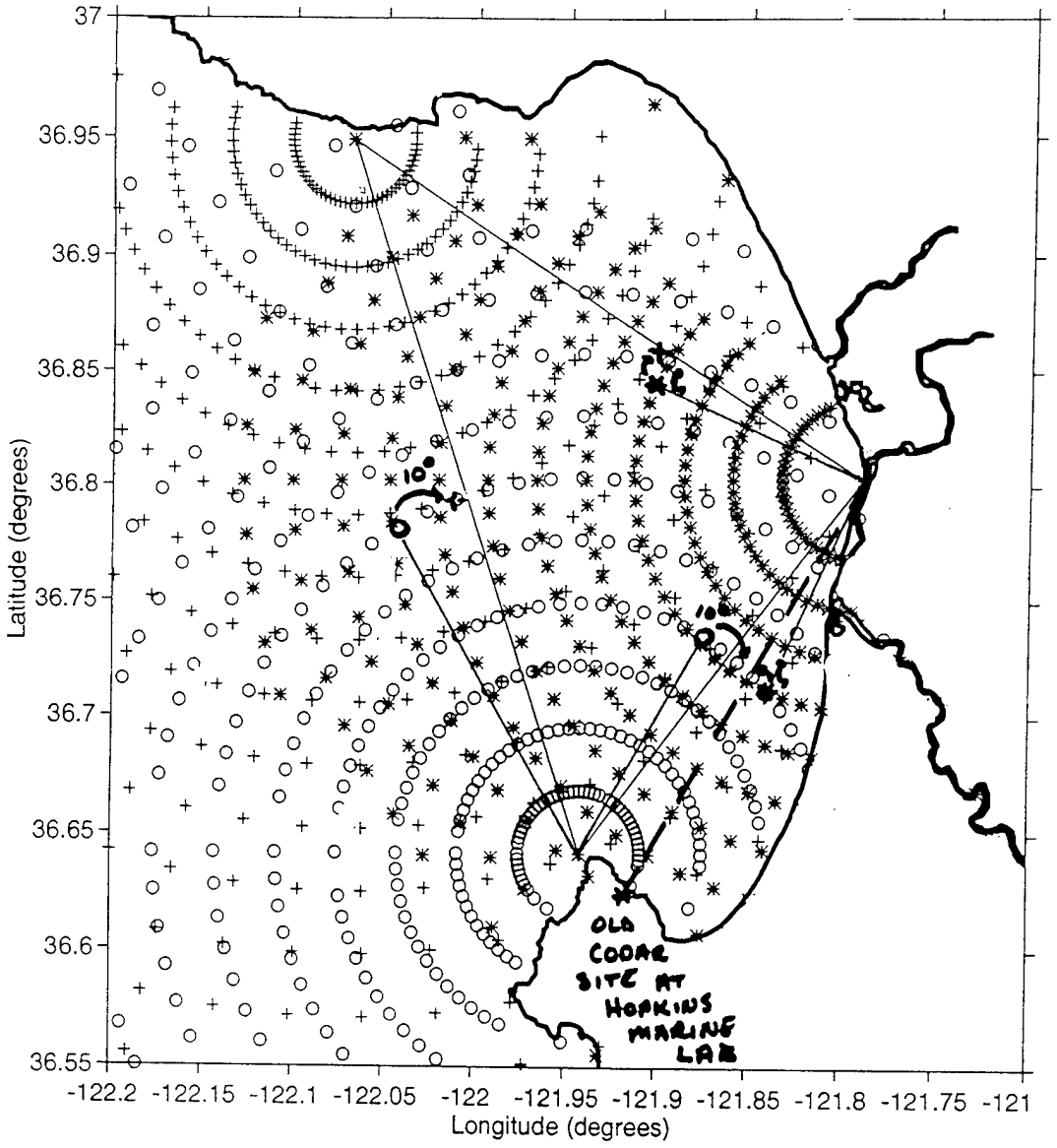

Figure 29. Illustration of the results of the baseline correlation and RMS difference analysis.

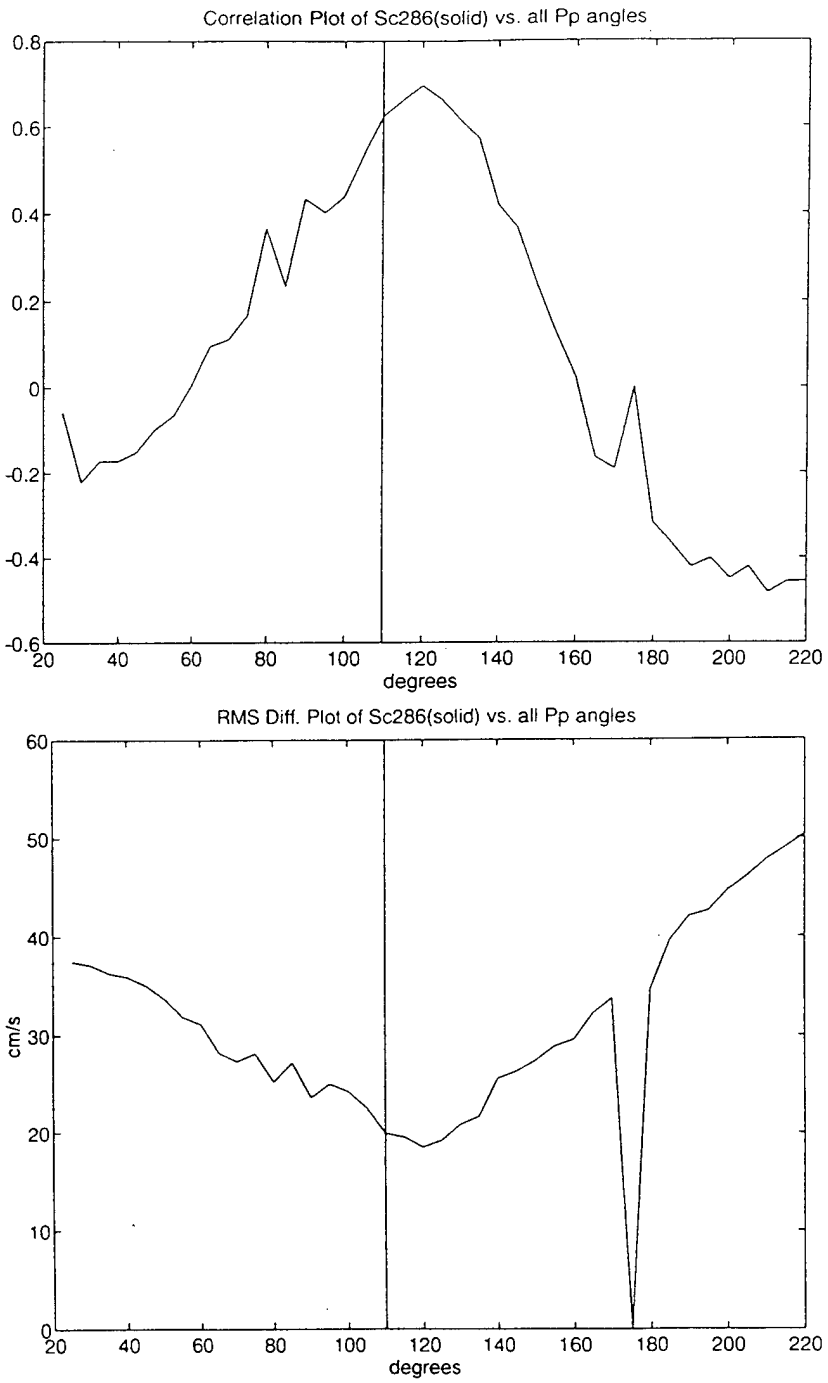

Figure 30. Correlation (upper panel) and RMS difference (lower panel) plots of 24 km baseline bin from the Santa Cruz SeaSonde site as compared to all radial 12 km bins from the Point Piños SeaSonde site. Results are plotted as a function of angle from the Point Piños site. Angle denoted by the vertical bar is the expected angle from the standard baseline pairs.

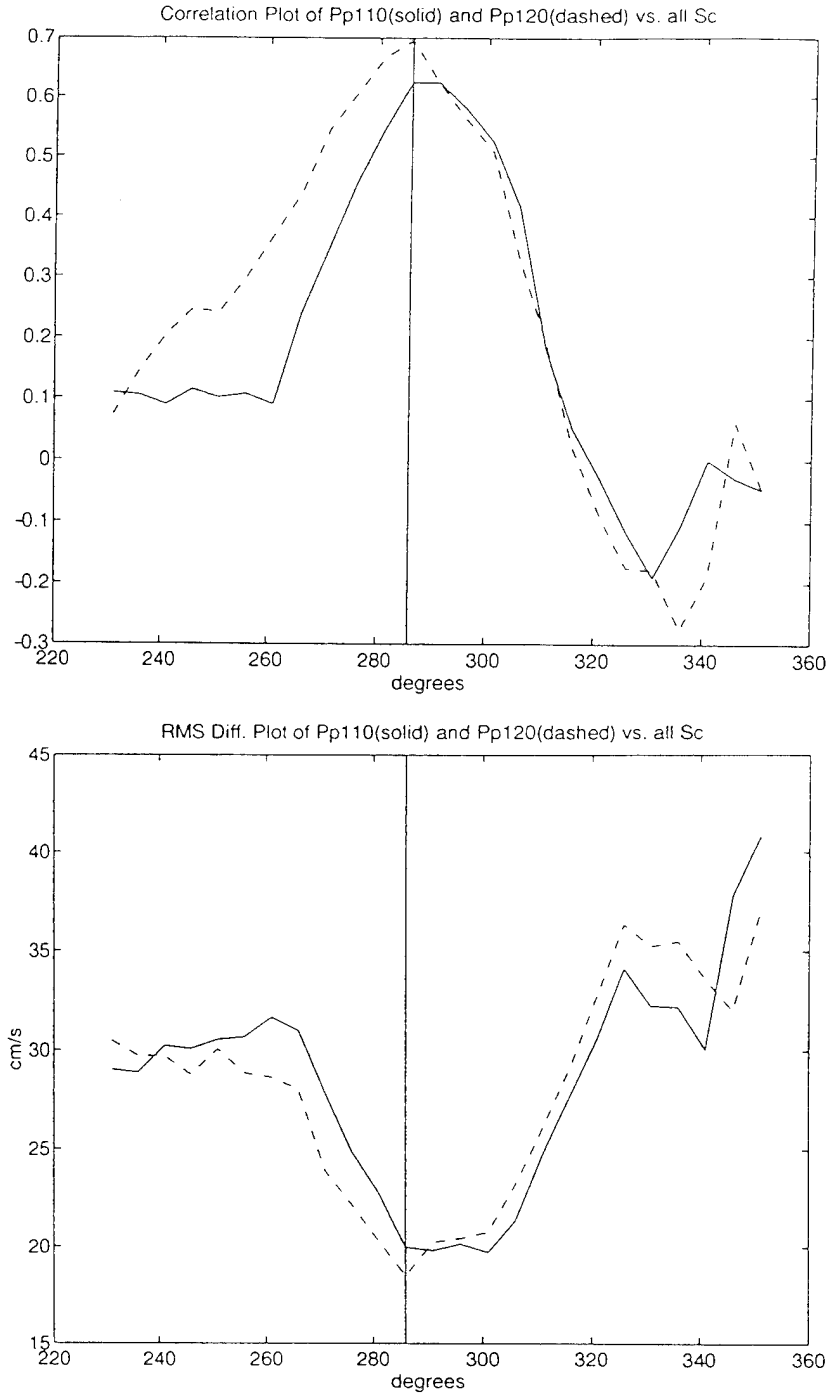

Figure 31. Correlation (upper panel) and RMS difference (lower panel) plots of the 12 km baseline bin from the Point Piños SeaSonde site as compared to all radial 24 km bins from the Santa Cruz SeaSonde site. Results are plotted as a function of angle from the Santa Cruz site for the standard (solid) and best correlated (dashed) gridpoint from Point Piños. Angle denoted by the vertical bar is the expected angle from the standard baseline pairs.

LIST OF REFERENCES

Barrick, D.E., Evans, M.W., and Weber, B.L., "Ocean Currents Mapped by Radar", *Science*, 198, pp. 138-144, 1977.

Barrick, D.E., Lipa, B.J., and Crissman, R.D., "Mapping Surface Currents with CODAR", *Sea Technology*, October, 1985.

Broenkow, W.W., and Smethie, W.M., Jr., "Surface Circulation and Replacement of Water in Monterey Bay", *Estuarine and Coastal Mar. Sci.*, 6, pp. 583-603,1978.

Crombie, D.D., "Doppler Spectrum of Sea Echo at 13.56 Mc/s", *Nature*, 175, pp. 681-682, 1955.

Essen, H.H., Gurgel, K.W., and F. Schirmer, "Surface Currents in the Norwegian Channel Measured by Radar in March 1985", *Tellus*, 41A, 162-174, 1989.

Foster, M.D., *Evolution of Diurnal Surface Winds and Surface Currents for Monterey Bay*, Master's Thesis, Naval Postgraduate School, Monterey, CA, 1993.

Lipa, B.J., and Barrick, D.E., "Least-Squares Method for the Extraction of Surface Currents from CODAR Crossed-Loop Data: Application at ARSLOE", *IEEE Journal of Oceanic Engineering*, OE-8, NO. 4, pp.226-253, 1983.

Neal, T.C., *Analysis of Monterey Bay CODAR-Derived Surface Currents*, March to May 1992, Master's Thesis, Naval Postgraduate School, Monterey, CA, 1992.

Paduan, J.D., Petruncio, E.T., Barrick, D.E., and Lipa, B.J., "Surface Currents Within and Offshore of Monterey Bay as Mapped by a Multiple-Site HF Radar (CODAR) Network", *Proceedings, IEEE Fifth Working Conference on Current Measurement*, pp. 137-142, February, 1995.

Paduan, J.D., and Rosenfeld, L.K., "Remotely Sensed Surface Currents in Monterey Bay from Shore-Based HF Radar (CODAR)", (submitted to) *Journal of Geophysical Research-Oceans*, 5 August 1995.

Petruncio, E.T., *Characterization of Tidal Currents in Monterey Bay from Remote and In-situ Measurements*, Master's Thesis, Naval Postgraduate School, Monterey, CA, 1993.

Stewart, R.H., and Joy, J.W., "HF Radio Measurement of Surface Currents", *Deep Sea Research*, 21, pp. 1039-1049, 1974.

INITIAL DISTRIBUTION LIST

		No. Copies
1.	Defense Technical Information Center Cameron Station Alexandria, VA 22304-6145	2
2.	Library, Code 013 Naval Postgraduate School Monterey, CA 93943-5101	2
3.	Dr. Robert H. Bourke (Code OC/BO) Department of Oceanography Naval Postgraduate School Monterey, CA 93943-5000	1
4.	Dr. Jeffrey Paduan (Code OC/PD) Department of Oceanography Naval Postgraduate School Monterey, CA 93943-5000	1
5.	Dr. Newell Garfield (Code OC/GF) Department of Oceanography Naval Postgraduate School Monterey, CA 93943-5000	1
6.	LT Darryl C. Melton, USN Surface Warfare Officer School Department Head Course Class 141 Newport, RI 02841	1
7.	Dr. Leslie Rosenfeld (Code OC/RO) Department of Oceanography Naval Postgraduate School Monterey, CA 93943-5000	1
8.	Director, Naval Oceanography Division Naval Observatory 34th and Massachusettes Avenue NW Washington, DC 20390	1
9.	Commander Naval Oceanography Command Stennis Space Ctr, MS 39529-5000	1
10.	Commanding Officer Naval Oceanographic Office Stennis Space Ctr Bay St. Louis, MS 39522-5001	1

11. Library 1
Scripps Institution of Oceanography
P.O. Box 2367
La Jolla, CA 92307

12. Library 1
Moss Landing Marine Lab
California State Colleges
Sandholdt Road
Moss Landing, CA 95039

13. Library 1
Hopkins Marine Station
Stanford University
Pacific Grove, CA 93950